Journal of Materials Research and Technology 30 (2024) 3485–3509

Contents lists available at ScienceDirect

Journal of Materials Research and Technology

journal homepage: www.elsevier.com/locate/jmrt

A new hybrid stretch forming and double-layer two-point incremental sheet forming process

Xuelei Zhao *, Hengan Ou **

Department of Mechanical, Materials and Manufacturing Engineering, Faculty of Engineering, University of Nottingham, NG7 2RD, UK

ARTICLE INFO

Keywords:
Incremental sheet forming
Stretch forming
Hybrid forming
Sheet thinning
Geometrical accuracy

ABSTRACT

This research presents a new hybrid stretch forming and double-layer two-point incremental sheet forming (hybrid stretch forming and DL-TPIF). The novelty of the proposed hybrid process is first to employ double-layer blank sheets in the conventional two-point incremental sheet forming (TPIF) process, which allows the material in the flange region to flow into the deformation region for achieving more uniform thickness distribution and less thinning. The use of an upper dummy sheet prevents the forming tool from direct contact the target blank sheet to improve the surface quality. Secondly, the combination of the stretch forming and the DL-TPIF processes enables seamless integration of the two forming processes to take advantages of both processes. The proposed new hybrid process was evaluated by two case studies through experimental testing and finite element (FE) simulation. Three pre-stretching conditions were examined to evaluate the effect of the prior stretching operation. The results showed that the maximum thickness reduction of the dome shape produced by the new stretch forming and DL-TPIF process was less than one third of that obtained from the conventional TPIF process. The geometrical accuracy and surface quality were also improved by using this new hybrid forming process.

1. Introduction

The incremental sheet forming (ISF) process has drawn significant attention over the last two decades. Due to its excellent adaptability and flexibility, the ISF process can be widely used in rapid prototyping and small-batch production of sheet products. The basic concept of the ISF process is to use a hemispherical forming tool moving along a predefined tool path and to deform the blank sheet into a designed product through gradual localised deformations of sheet materials. The motion of the hemispherical forming tool is controlled by a computer numerical controlled (CNC) milling machine [1,2]. Easy control of the tool motion and no need for forming dies or complex tooling make the ISF process cost-effective and easy to operate. Although the ISF process is an emerging flexible sheet forming process with many advantages for potential industrial implementations, there are limitations, including poor surface quality, excessive sheet thinning, low geometrical accuracy, limited maximum draw angle, and long forming time [3,4]. These drawbacks hinder the further development of the conventional ISF process. In recent year, hybrid sheet forming processes in combining the ISF process with other sheet forming processes investigated and shown as a promising solution to overcome the limitations of the conventional ISF processes.

Araghi et al. [5] proposed the hybrid stretch forming and ISF process, in which the stretch forming process was used as a pre-forming operation, and a subsequent two-point incremental sheet forming (TPIF) process was implemented to complete the final forming procedure. TPIF is one of the conventional ISF processes in which a partial or full die is used to support the blank sheet during the forming operation [6]. Many studies have been conducted to investigate this hybrid process. Compared to the conventional ISF processes, improvements can be made in achieving reduced forming time, uniform thickness variations, and improved geometrical accuracy [7–9]. Araghi et al. [10] produced an irregular part with a mild steel DC04 sheet to study the effects on the forming time. The experimental results showed that the forming time with the conventional TPIF process was 60 min, as compared to 40 min with the hybrid process. The surface area covered by the tool path determined the TPIF process forming time. And the stretch forming time was commonly scaled by the designed profile height, as the stretch forming was faster than the conventional TPIF process when producing a part without special features (e.g., pocket and groove features). Araghi

* Corresponding author.
** Corresponding author.
E-mail addresses: Xuelei.Z@outlook.com (X. Zhao), h.ou@nottingham.ac.uk (H. Ou).

https://doi.org/10.1016/j.jmrt.2024.04.093
Received 29 November 2023; Received in revised form 3 April 2024; Accepted 11 April 2024
Available online 12 April 2024

et al. [5] and Choi and Lee [11] experimentally compared the thinning effects of the conventional TPIF and the hybrid stretch forming and TPIF processes by creating a spherical cap with a groove and the bottom surface of the ship panel, respectively. The results showed that a more uniform thickness distribution with less thinning could be obtained by this hybrid process as compared to the conventional TPIF process. This can be explained by the different material deformation modes between the stretch forming and conventional TPIF processes. The stretch forming process could induce thinning in regions that are not deformed by the TPIF process. Araghi et al. [12] investigated the effect of this hybrid process on the geometrical accuracy by producing a hydraulic access door panel for the Airbus A320 with a 1 mm mild steel DC04. The author found that the maximum deviation was reduced from 3.3 mm by the conventional TPIF process to 1.3 mm by using the hybrid process. Lora et al. [13] carried out experimental testing and finite element simulations to study the formability limits of the hybrid stretch forming and TPIF process. It was found that higher levels of pre-deformation resulted in lower subsequent major true strains during the TPIF process. The hybrid forming process enables the production of sheets with larger minor true strains, contributing to greater homogeneity in the formed sheets. Since the TPIF process primarily involves planar deformations, the hybrid forming process expands design possibilities further. In addition to the hybrid stretching forming and TPIF process, Lu et al. [14] proposed a two-stage hybrid ISF that combines stretch forming with the single-point incremental sheet forming (SPIF) process. In contrast to the TPIF process, where there is a backup die supporting the blank sheet, the SPIF process may be characterised by the motion of a hemispheric tool that makes a single point contact with the blank sheet. The hybrid stretch forming and SPIF process is also a two-stage forming process. It was different from the hybrid stretch forming and TPIF processes, in which the flange region was clamped rigidly. In this case, since the edge of the target blank sheet was not fully constrained, more material was allowed to flow into the deformation region during the stretch forming stage. Therefore, the sheet thinning was significantly reduced, and higher formability would be achieved than that of the conventional ISF process. The second stage was the SPIF process, which was used to complete the remaining forming operations. Zhang et al. [15] validated this flexible hybrid process through a hemisphere case study. The initial thickness of the sheet was 0.8 mm. The minimum thickness was 0.68 mm for the part produced by the hybrid forming process as compared to a minimum thickness of 0.46 mm obtained by the conventional SPIF process.

In order to improve the surface quality of the final product, Skjoedt et al. [16] first suggested using an upper dummy sheet when conducting the SPIF process in 2007. The upper dummy sheet was implemented to avoid the forming tool being in direct contact with the target blank sheet, so it could significantly eliminate tool marks and improve the surface finish. However, the basic mechanism of sheet deformation was essentially the same as the conventional ISF process, as the common problem in sheet thinning is still yet to be addressed. A three-sheet incremental sheet forming process was proposed by Chang et al. [17], in which the target blank sheet was placed between upper and lower dummy sheets. The authors conducted finite element simulations to investigate the deformation mechanisms. The authors found that the lower dummy sheet offered additional compressive stress to the target blank sheet that decreased the stress triaxiality on the deformed part, which could delay crack growth and enhance process formability. Based on the three-sheet incremental sheet forming process, Chang et al. [18] developed the flexible free ISF process, and three sheets were also employed in this forming process. It was different from the above three-sheet incremental sheet forming process in which the target blank sheet was deformed without any edge constraint in the flexible free ISF process. The results showed that a part without extremely thinned regions could be produced by this hybrid forming process. As compared to

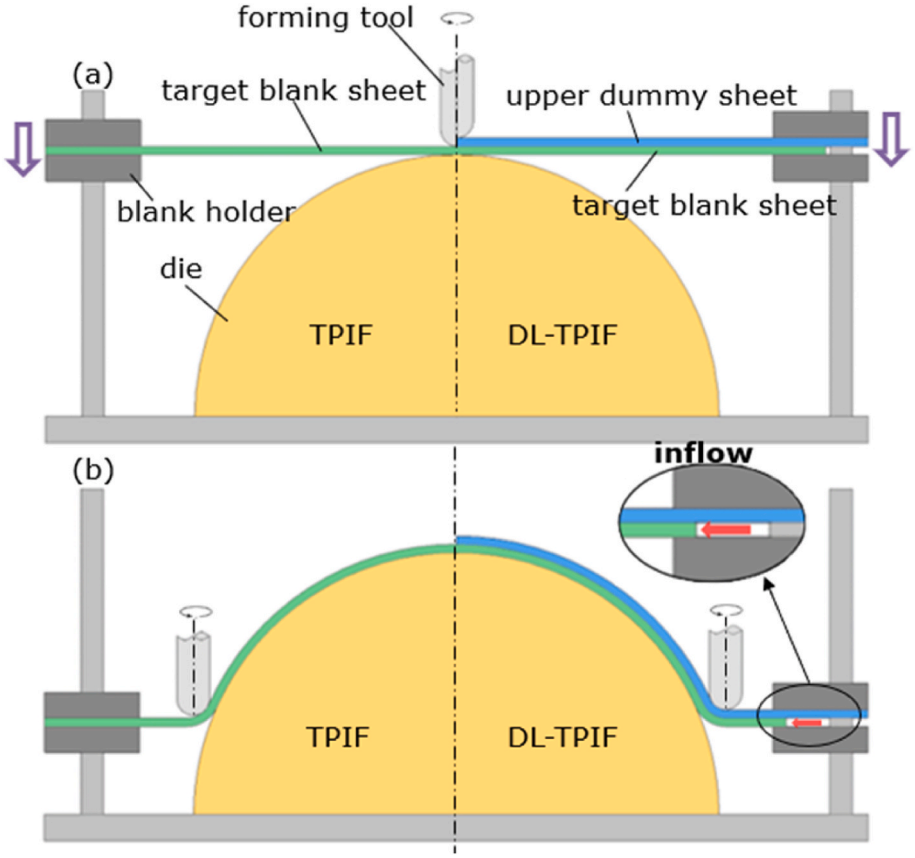

Fig. 1. Comparisons between the conventional TPIF and the new DL-TPIF processes: (a) the initial state and (b) the end of forming operations.

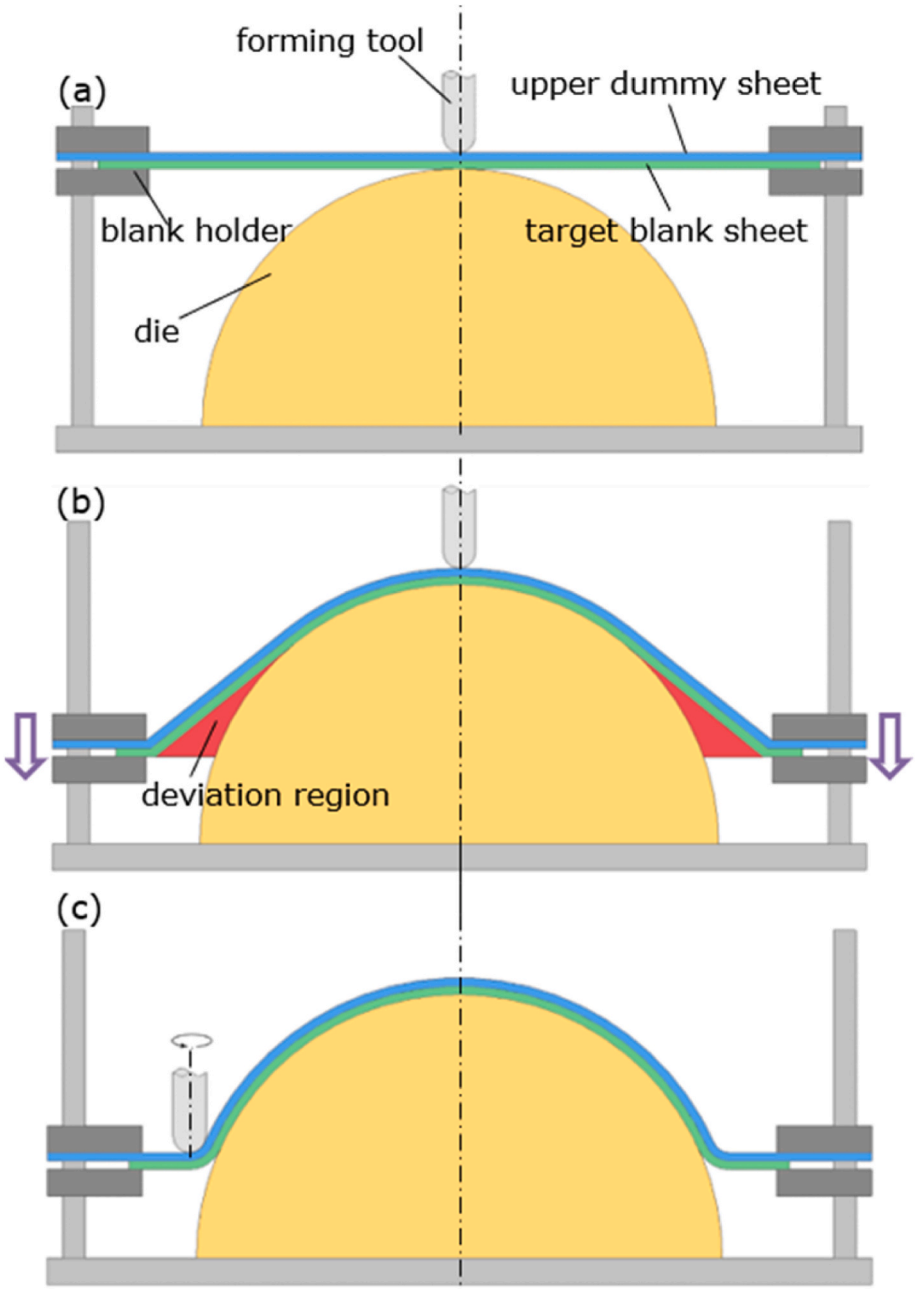

Fig. 2. Hybrid stretch forming and DL-TPIF process, (a) initial state (b) first stage: stretch forming (c) second stage: DL-TPIF process.

the conventional ISF process, the flexible free ISF process could achieve more uniform thickness distribution, better geometrical accuracy, and smoother surface quality. Zhao and Ou [19] created a new flexible multi-point incremental sheet forming process with multi-layer sheets. A new flexible multi-point die system was devised to ensure the multi-point pins are in contact with and support the blank sheet during the whole forming operation. Additionally, the use of multi-layer sheets enables the target blank sheet to be deformed without constraints. The authors found that the maximum thickness reduction is significantly reduced from 35% to 5% as compared to the conventional multi-point incremental sheet forming process when producing a dome shape, and more uniform thickness distributions and better surface quality could be achieved. The results also showed a noticeable reduction of wrinkling by using the new flexible multi-point die over the conventional multi-point die system with multi-layer sheets in forming a dome shape. The authors conducted finite element analysis to study the wrinkling behaviour, and explained that the flexible multi-point pins keep direct contact with the blank sheet, the through-thickness stress was higher than that when using the conventional multi-point die, which provided normal pressure to suppress wrinkling. Overall, it can be concluded that releasing the clamping constraints to the target blank sheet is an effective approach to overcome the sheet thinning issue in ISF processing.

However, in the current hybrid stretch forming and TPIF process, the target blank sheet is clamped rigidly by the blank holders. It is still challenging to allow the amount of material in the clamping area to be drawn into the deformation region in one setup. Moreover, when combining the stretch forming and ISF processes, the ISF process is normally conducted after the full stretch forming operation. Therefore, in this research, a new variant of the hybrid process was proposed: the hybrid stretch forming and double-layer incremental sheet forming (hybrid stretch forming and DL-TPIF) process. The main concept of this proposed hybrid process is twofold. The first is to employ double-layer

blank sheets instead of the single blank sheet in the conventional TPIF process. The target blank sheet is placed between the upper dummy sheet and the supporting die. As it is not rigidly clamped, the target blank sheet can be drawn into the deformation region. Therefore, a part with less thinning, a more uniform thickness distribution, and better surface quality can be produced by the proposed DL-TPIF process. The second is to incorporate the stretch forming process as a pre-forming step. The combination of the stretch forming and DL-TPIF processes enables seamless integration of the two separate operations to obtain the advantages of both forming processes.

To evaluate the proposed hybrid stretch forming and DL-TPIF process through experimental testing and FE simulations, two case studies (dome shape and irregular shape) were carried out to investigate the effect of pre-stretching conditions and compare the performance of employing double blank sheets to the conventional TPIF process in terms of strain and stress distributions, thickness variations, and geometrical accuracy. The concepts of the proposed hybrid stretch forming and DL-TPIF process are provided in Section 2. The experimental setup is presented in Section 3. Section 4 focuses on FE modelling. Experimental testing and FE predicted results under different forming conditions are discussed in Section 5. Finally, the findings of this research are presented in Section 6.

2. Concepts of the new hybrid stretch forming and double layer two-point incremental sheet forming process

2.1. DL-TPIF process

In the conventional ISF processes, the blank sheet is clamped rigidly by the blank holders, so the blank sheet is deformed without the flow of material from the clamping region. The concept of the double-layer two-point incremental sheet forming (DL-TPIF) process is proposed to allow the material in the clamping area to be drawn into the deformation region. The comparisons between the conventional TPIF and the proposed DL-TPIF processes are presented in Fig. 1. In the conventional TPIF process, the blank sheet is deformed against a supporting die. The combination of the blank holder vertical motion and the ISF tool motion via a defined trajectory allows the desired shape to be formed. In the proposed DL-TPIF process, except for the upper dummy sheet, the basic setup and forming procedure are similar to the conventional TPIF process. The target blank sheet is placed between the supporting die and the upper dummy sheet. In the previous TPIF process with a dummy sheet proposed by Li et al. [20], the dummy sheet was also placed above the target blank sheet, and both were fully clamped by the blank holders. However, in the proposed DL-TPIF process, the material from the target blank sheet is not rigidly clamped in the clamping area, so it allows the blank sheet material to flow into the deformation, as shown in Fig. 1 (b).

2.2. Hybrid stretch forming and DL-TPIF process

Fig. 2 shows the concept of the proposed new hybrid stretch forming and DL-TPIF process. This new hybrid process involves two stages. A stretch forming process is followed by the DL-TPIF process. As presented in Fig. 2 (b) and (c), the stretch forming process may not produce the whole designed profile. The subsequent DL-TPIF process is performed to complete the forming operation. Compared to the previous hybrid stretch forming and TPIF process proposed by Araghi et al. [5], this new hybrid process employs the DL-TPIF process instead of the conventional TPIF process, which allows material in the clamping area to flow into the deformation region.

The following advantages are expected from the proposed hybrid stretch forming and DL-TPIF process.

- **Reduced sheet thinning and thickness variation**

The target blank sheet is not fully clamped, which allows the material from the clamping area to draw into the deformation region. With the material supplement, a formed sheet part with less thinning and more uniform thickness distribution is expected when conducting the DL-TPIF process as compared to the conventional TPIF process. In addition, the deformation modes and maximum thinning regions between the stretch forming and DL-TPIF processes are different. For instance, when producing a dome shape, the maximum thinning occurs in the central region, and the sheet thinning decreases in the radial direction after the maximum thinning in the case of the stretch forming process. In contrast to the stretch forming process, the sheet thickness decreases with the increased draw angles in the DL-TPIF process. Hence, combining the stretch forming and DL-TPIF processes offers the possibility of obtaining a better thickness distribution than the conventional TPIF process.

Table 1
Six forming processes for experimental testing and FE analysis.

Forming processes			Stretch forming depth (mm)	Experiment	FE
P1	TPIF	Conventional	0	✓	✓
P2		SF + TPIF	15	✓	✓
P3		SF + TPIF	Full	×	✓
P4	DL-TPIF	Conventional	0	✓	✓
P5		SF + DL-TPIF	15	✓	✓
P6		SF + DL-TPIF	Full	×	✓

- **Improved surface quality**

In the new hybrid process, a piece of dummy sheet is placed over the target blank sheet. The dummy sheet is implemented to avoid the forming tool being in direct contact with the target blank sheet, so it can significantly eliminate tool marks and improve the surface quality of the final product.

- **Improved geometrical accuracy**

A supporting die is employed in this hybrid process. Compared to the conventional dieless SPIF process, the use of a die can better control the localised deformation and achieve a smaller amount of springback upon unloading. Hence, better geometrical accuracy can be obtained. Additionally, due to the superimposed tension stresses caused by the stretch forming process, the combination of stretch forming and DL-TPIF processes can produce a higher degree of dimensional accuracy than that of the conventional TPIF process.

3. Experimental testing

In order to demonstrate the new concept of the DL-TPIF process and investigate the advantages of the new hybrid stretch forming and DL-TPIF processes, six forming processes were carried out under different operational conditions, as listed in Table 1. These six forming processes were divided into two categories based on the number of blank sheet layers used in the forming operation (e.g., TPIF and DL-TPIF processes). Stretch forming can be applied in different sequences: before the TPIF (or DL-TPIF) processes, it is called “pre-stretching”, and during the TPIF (or DL-TPIF) processes, it is called “in-process stretching”. In order to investigate the effect of conducting the stretch forming process, three pre-stretching conditions were considered in this study, including 0 mm, 15 mm, and full depth. Due to the capacity of the lifting machine, only 15 mm of the pre-stretching operation could be conducted for the experimental testing.

According to Fig. 3 (a), the 0 mm pre-stretching condition indicates that no stretch forming process is implemented. Under this condition, the part is produced only by either the TPIF or DL-TPIF processes. In the second pre-stretching condition, as presented in Fig. 3 (b), the stretch forming is first carried out to a depth of 15 mm, and then the ISF forming

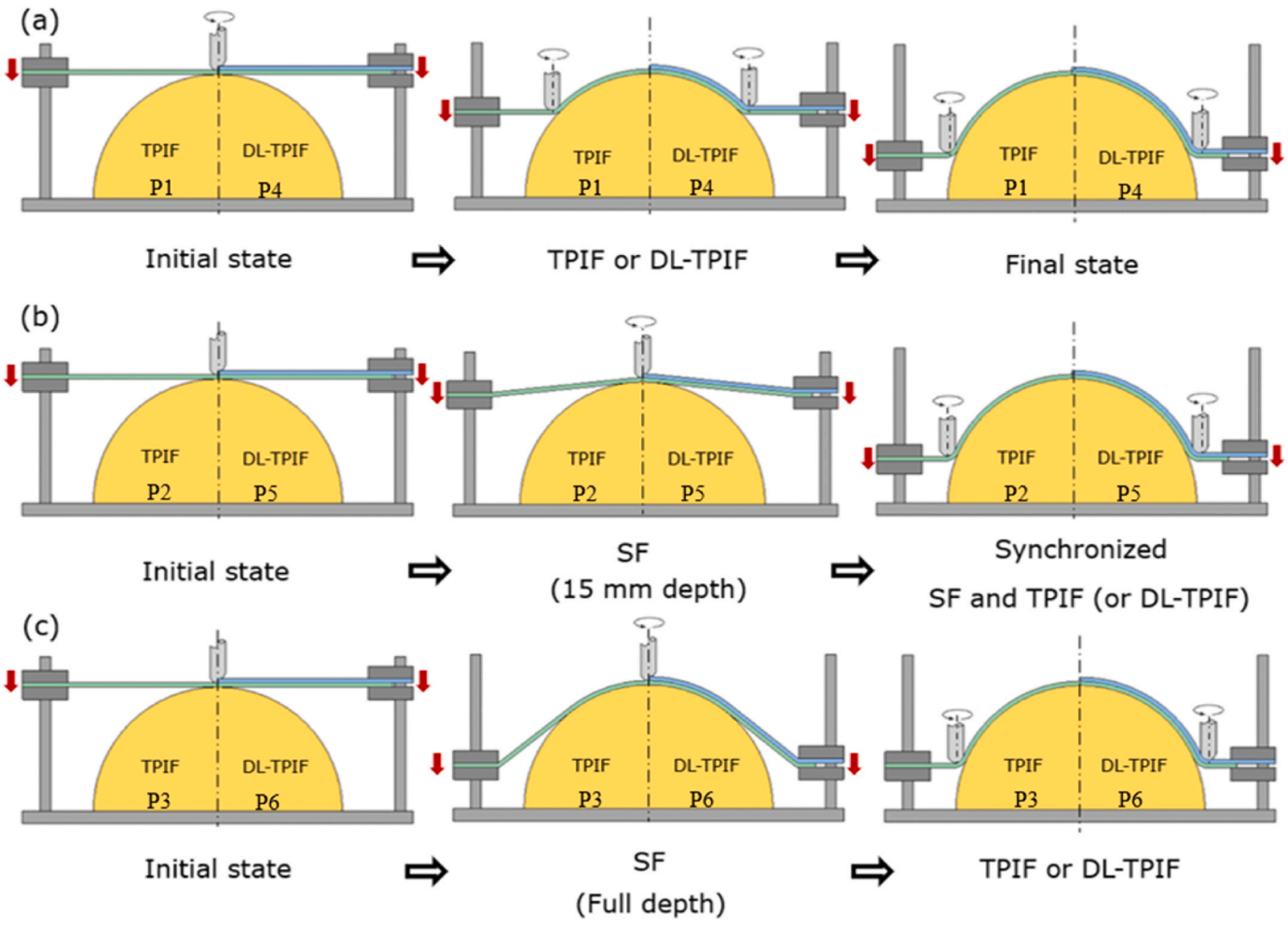

Fig. 3. Hybrid stretch forming and TPIF (or DL-TPIF) processes under different pre-stretching conditions: (a) 0 mm, (b) 15 mm, and (c) full SF.

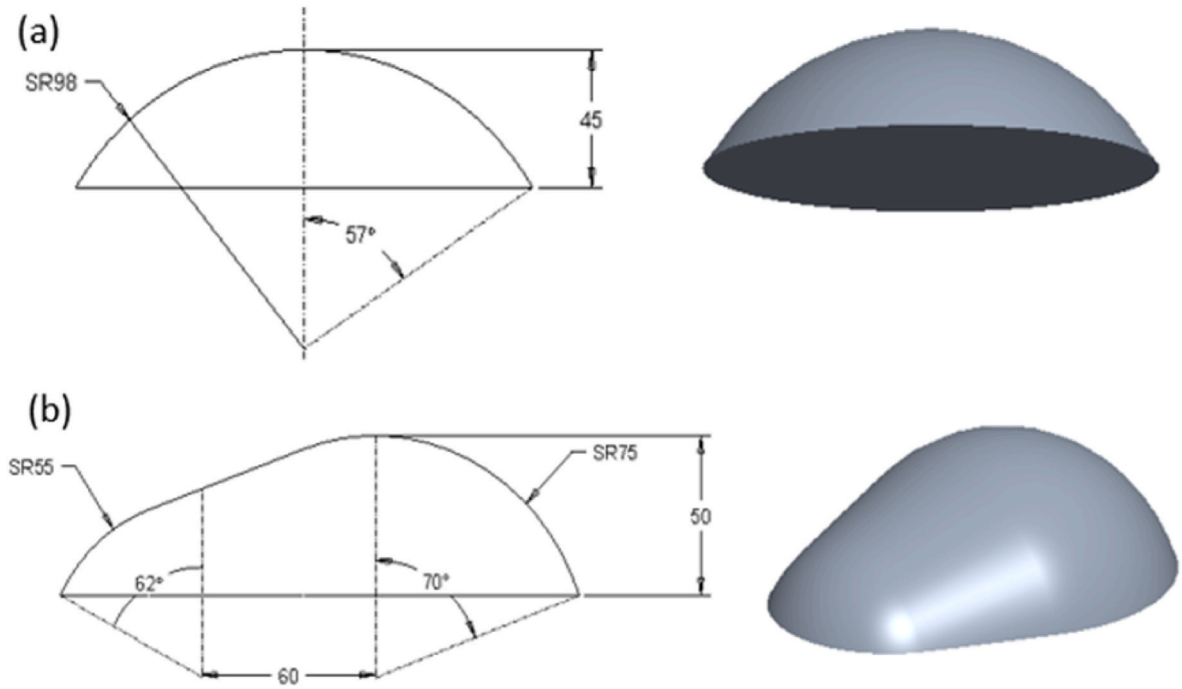

Fig. 4. Designed profiles of (a) dome case with 57° draw angles, and (b) irregular case with 70° draw angles.

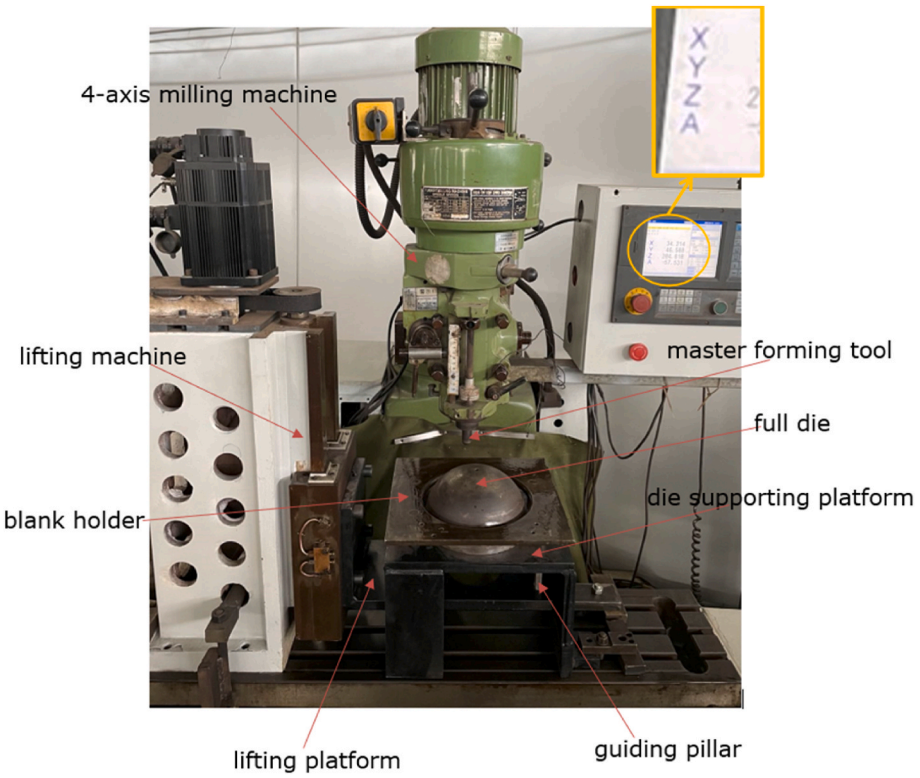

Fig. 5. The experimental set-up for the new hybrid stretch forming and DL-TPIF process.

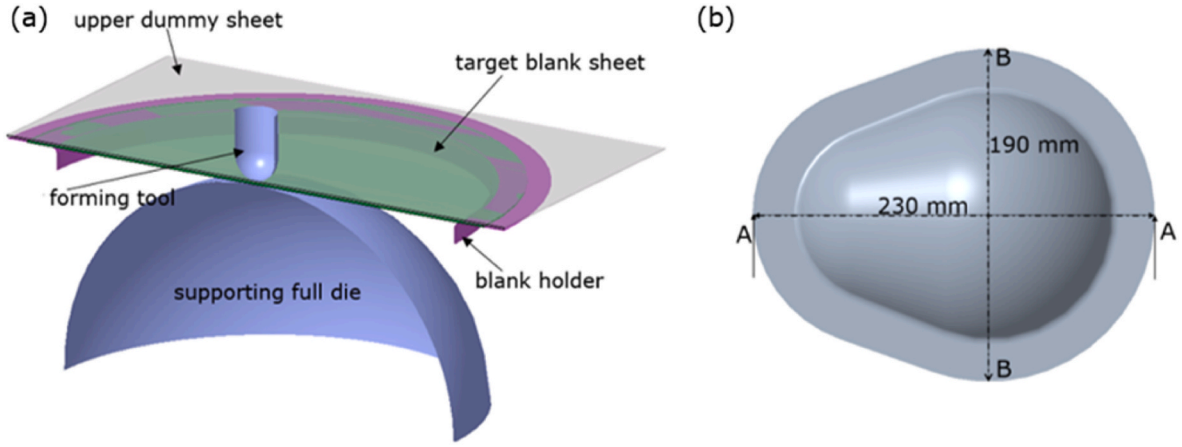

Fig. 6. (a) Sectional view of the DL-TPIF process basic setup for the dome case; (b) profile of target workpiece of irregular shape.

tool starts to move along the designed tool path of the TPIF (or DL-TPIF) process together with the stretch forming operation towards the end of the hybrid forming process. This enables the stretch forming and TPIF (or DL-TPIF) processes to conduct synchronously after the pre-stretching step. From Fig. 3 (c), the full pre-stretching depth condition means that the TPIF (or DL-TPIF) process is carried out after the full stretch forming process to complete the forming operation. As a result, the stretch forming and TPIF (or DL-TPIF) processes are conducted sequentially.

Two case studies were investigated to demonstrate the proposed hybrid stretch forming and DL-TPIF process. The first case was a dome shape with a 57° draw angle, and the second was an irregular profile with a 70° draw angle, as shown in Fig. 4.

Fig. 5 shows the experimental setup to carry out the testing for the hybrid stretch forming and DL-TPIF process. A 4-axis milling machine was used to control the motions of the X, Y, and Z-axis of the forming tool. An extra A-axis was employed to control the lifting machine that drove the blank holders down and up. The movements of the forming tool and blank holders were controlled separately. When conducting the pre-stretching operation, the lifting machine drove the metal sheet downward until it reached the desired stretch forming depth. And then, the forming tool started to move along the defined toolpath.

The forming tool used for all experiments had a hemispherical head with a 10 mm diameter. According to Zhang et al. [15], 10 mm in diameter was a reasonable choice for the forming tool to achieve a good level of formability in the ISF process. A helical tool path with a constant step size of 0.5 mm and a feed rate of 200 mm/min was employed. The metal sheet was a steel DC01 sheet with 0.8 mm thickness. A soft, low melting-point paste lubricant, Rocol RTD Compound, was applied to all contact surfaces.

The core of the proposed DL-TPIF process is that the target blank

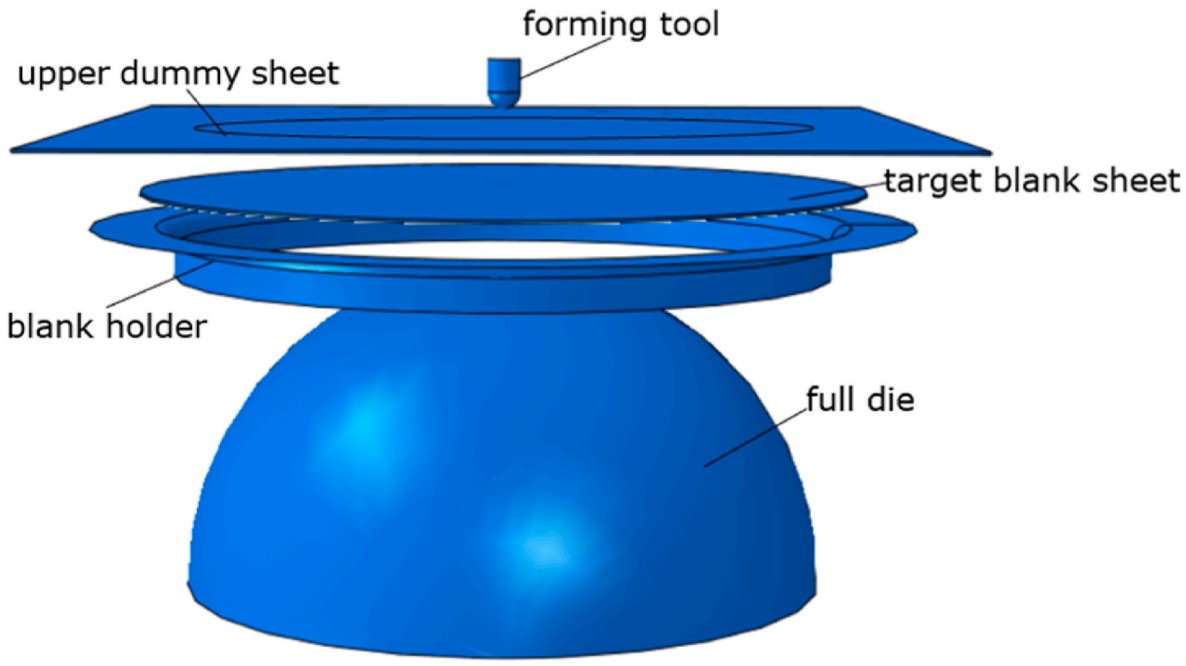

Fig. 7. FE models for the dome shape by the DL-TPIF or hybrid stretch forming and DL-TPIF processes.

sheet is allowed to move along the drawing direction, but the upper dummy sheet is clamped rigidly by the blank holders. Under this arrangement, the upper dummy sheet and blank holder sizes should be larger than the target blank sheet, as presented in Fig. 6 (a). Therefore, in the case of the dome shape, the diameter of the target blank sheet was 250 mm, while the size of the upper dummy sheet was 300 × 300 mm. In the case of the irregular shape, the initial profile of the target blank sheet should depend on the final product geometry, which allows the material in the clamping area to be drawn into the deformation region smoothly and evenly. Hence, the initial target blank sheet was trimmed into an irregular shape, as shown in Fig. 6 (b). And the size of the upper dummy sheet was 300 × 300 mm.

4. Finite element modelling

ABAQUS/Explicit was used to conduct the FE simulations to predict the material behaviour of the metal sheet. This section presents the details of FE modelling for the hybrid stretch forming and DL-TPIF process. In order to establish a clear insight into the proposed new hybrid forming process, the simulation results were compared to the conventional TPIF process in terms of strain and stress distributions, thickness variations, and geometrical accuracy. The method to determine the predicted thickness distributions and geometrical accuracy from FE simulations was also included in this section.

As shown in Table 1, six FE models were developed for each case study, which included the stretch forming, TPIF, and DL-TPIF processes. The basic components involved in the TPIF, and hybrid stretch forming and TPIF processes include a forming tool, target blank sheet, and a full die. An extra upper dummy sheet and a blank holder were adopted in the FE models of the proposed DL-TPIF, and hybrid stretch forming and DL-TPIF processes, as shown in Fig. 7. In order to save commutating time, the target blank sheet in the TPIF process, and the upper dummy sheet in the DL-TPIF process were partitioned into two regions: the clamping region and the deformation region. Hence, it was more efficient to constrain the clamping regions of the sheet rather than employ an extra upper blank holder to limit the movement of the sheets.

The forming tool, blank holder, and full rigid die were modelled as district rigid shell bodies using R3D4 element, which is a four-node 3D linear rigid quadrilateral element. The forming tool was finely meshed

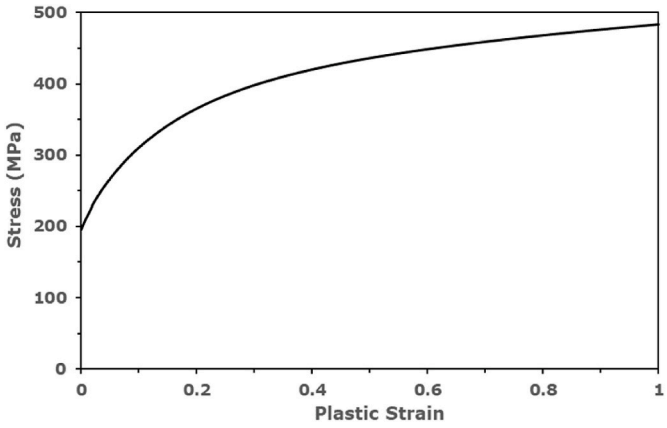

Fig. 8. DC01 Steel sheet plastic stress-strain curve for FE modelling.

with an element size of 0.5 mm to allow smooth curvature, while the blank holder and full rigid die mesh size were 2 mm. In the dome case, both the dummy sheet and target blank sheet were modelled by using eight-node brick elements with reduced integration (C3D8R). Six-node wedge elements (C3D6) were used in the irregular case to mesh the blank sheets. The approximate size was 2 mm, and there were three elements along the thickness direction.

DC01 steel sheet with a 0.8 mm initial thickness was employed as the dummy and target blank sheet material. Young's modulus of 208 GPa and Poisson's ratio of 0.267 were used to define material properties. Tensile tests were carried out to obtain the strain-stress flow curve in this work. The flow stress curve of the DC01 steel sheet adopted in FE modelling is shown in Fig. 8.

A global friction coefficient of 0.05 [21] was applied in these FE simulations. This value was widely used in the ISF process FE analysis with steel DC01 sheet, and the simulation results correspond well to the experimental results obtained by Aerens et al. [22]. A helical tool path with a constant step size of 0.5 mm and a feed rate of 200 mm/min was used in this analysis. Mass scaling has been used in this study to reduce computing time. The mass scaling factor may lead to error or failure of

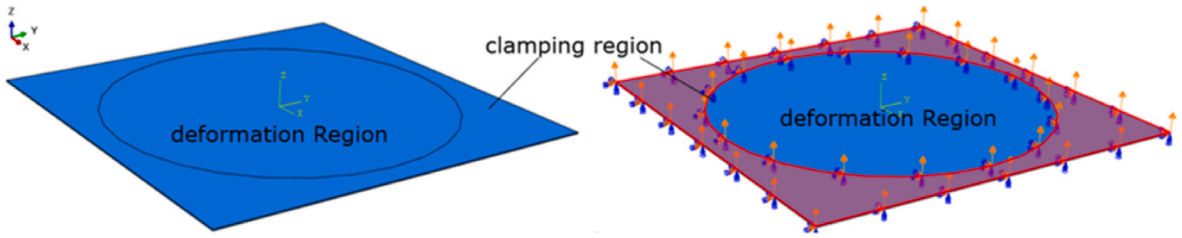

Fig. 9. Boundary conditions for the blank sheet.

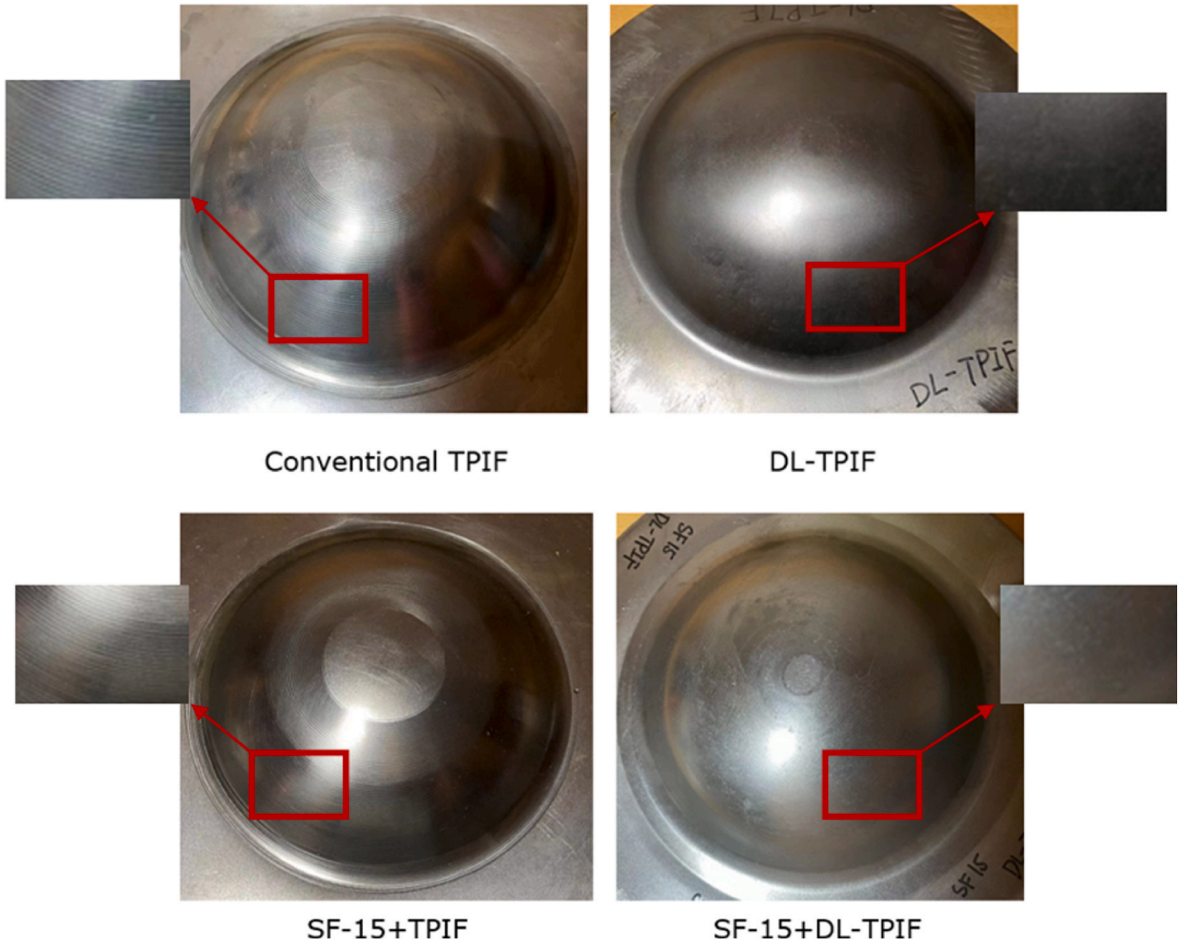

Fig. 10. Experimental results for the dome case.

the simulation due to the fact that kinetic energy can be raised if a large value of mass scaling is selected. However, using a small value of mass scaling could result in a lengthy computation time. Thus, a consistent time increment of $2 \times 10^{-5}s$ was employed to guarantee that relative values between kinetic and internal energy are within the range of less than 0.4%–10%.

In terms of boundary conditions, the rigid full die was fixed on all axes for the six FE models. In the conventional TPIF process, the forming tool was controlled by its reference point and moved along the assigned tool path. As shown in Fig. 9, the target blank sheet was partitioned into clamping and deformation regions, so the displacement for the blank holder was applied to the clamping region. The blank sheet could only move vertically, and its motions should be identical to those of the forming tool in the Z direction.

In the DL-TPIF process, two pieces of blank sheets were adopted, and the top blank sheet was used as a dummy sheet, which was placed above the target blank sheet. The clamping region of the upper dummy sheet and the lower blank holder could only move downward and follow the same movement as the forming tool in the Z direction. The edge boundary condition for the target blank sheet was set as free, but it was clamped by the upper dummy sheet and lower blank holder. In such a case, the blank sheet could be driven and moved down synchronously. At the same time, the clamping region of the target blank sheet was not rigidly clamped, which allows relative sliding between the sheets.

There were two stages in both the hybrid stretch forming and TPIF, and the hybrid stretch forming and DL-TPIF processes. The first stage was the pre-stretching operation, in which a certain displacement was applied to the clamping region of the blank sheet or the upper dummy sheet. So, the clamping region was stretched to a certain depth, and the sheet was deformed against a full die. In the second stage, the TPIF or DL-TPIF process was started by the defined tool path motion of the forming tool. If the pre-stretching depth was less than the full-depth condition, the stretch forming process was required to be conducted synchronously with the TPIF (or DL-TPIF) process. Therefore, in

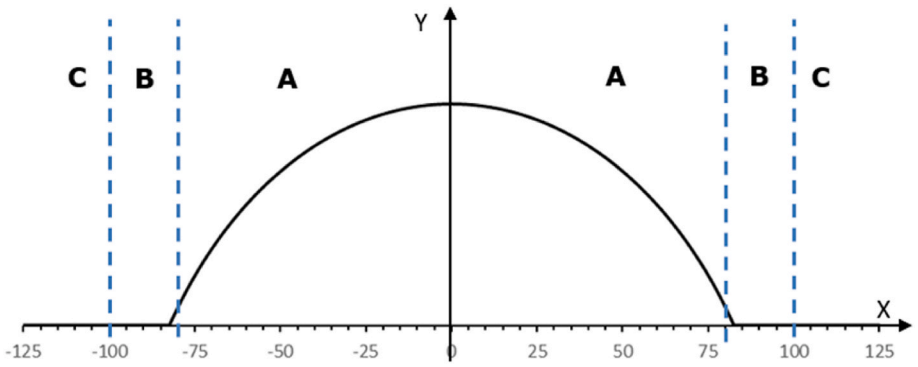

Fig. 11. Meridional cross-section for measurements and a schematic of region divisions for the dome case.

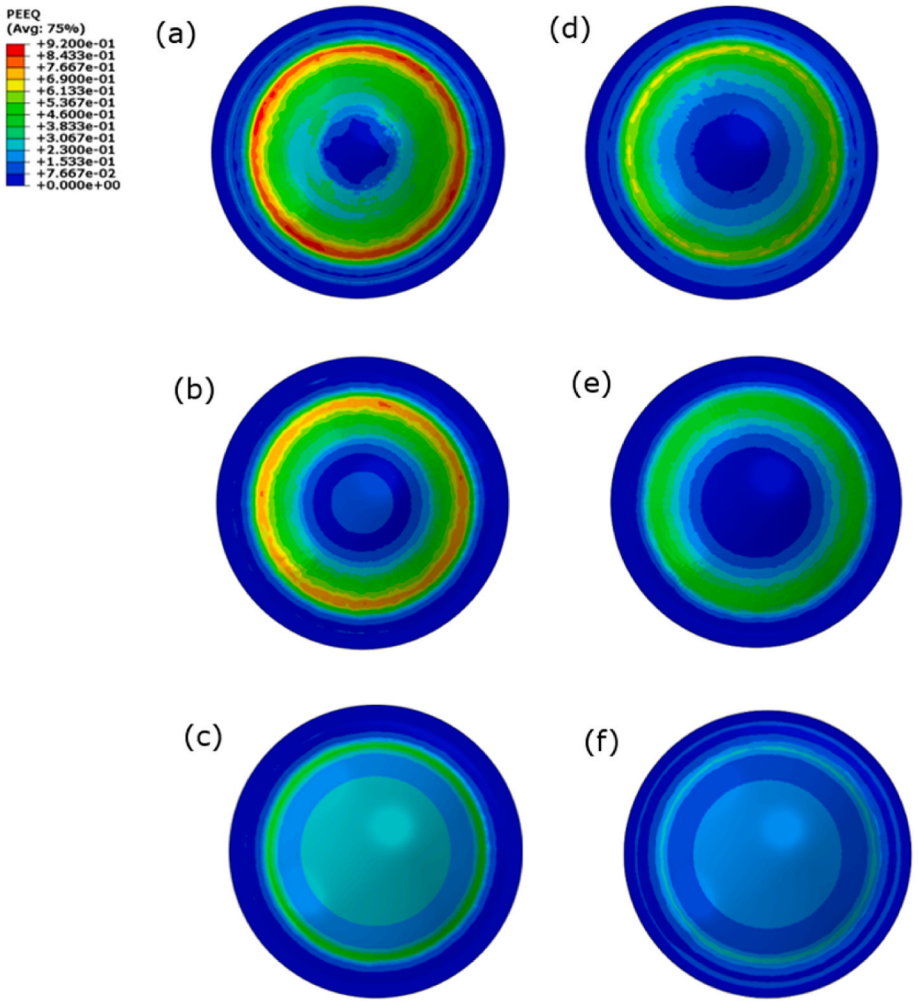

Fig. 12. Equivalent plastic strain distributions obtained from FE simulations produced by (a) TPIF, (b) SF-15 + TPIF, (c) SF-full + TPIF, (d) DL-TPIF, (e) SF-15 + DL-TPIF, (f) SF-full + DL-TPIF processes.

combining the stretch forming and TPIF (or DL-TPIF) processes, the blank sheet always reached the designed position before the forming tool for the TPIF (or DL-TPIF) processes.

5. Results and discussion

5.1. Case 1: dome shape

A dome shape with a 57° draw angle was employed in this investigation, as illustrated in Fig. 4 (a). The final tested deformed parts are shown in Fig. 10. It was obvious that tool marks were observed in the parts produced by the conventional TPIF and hybrid stretch forming and TPIF processes. The tool trajectory marks induced by tool squeezing applied to the blank sheets caused higher contact pressure and greater friction. In the DL-TPIF process, the upper dummy sheet prevented the forming tool from directly contacting the target blank sheet. Thus, fewer tool marks were found, and the surface quality improved significantly.

The experimental testing and FE predicted results were compared in

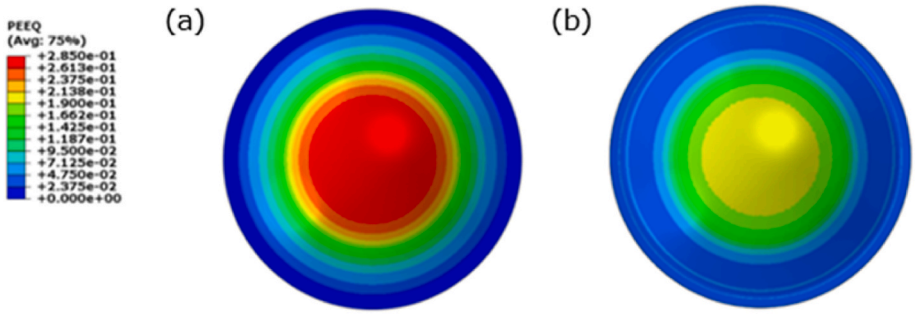

Fig. 13. PEEQ distributions after the full stretch forming process under different operational conditions: (a) TPIF with 45 mm of SF, (b) DL-TPIF with 45 mm of SF.

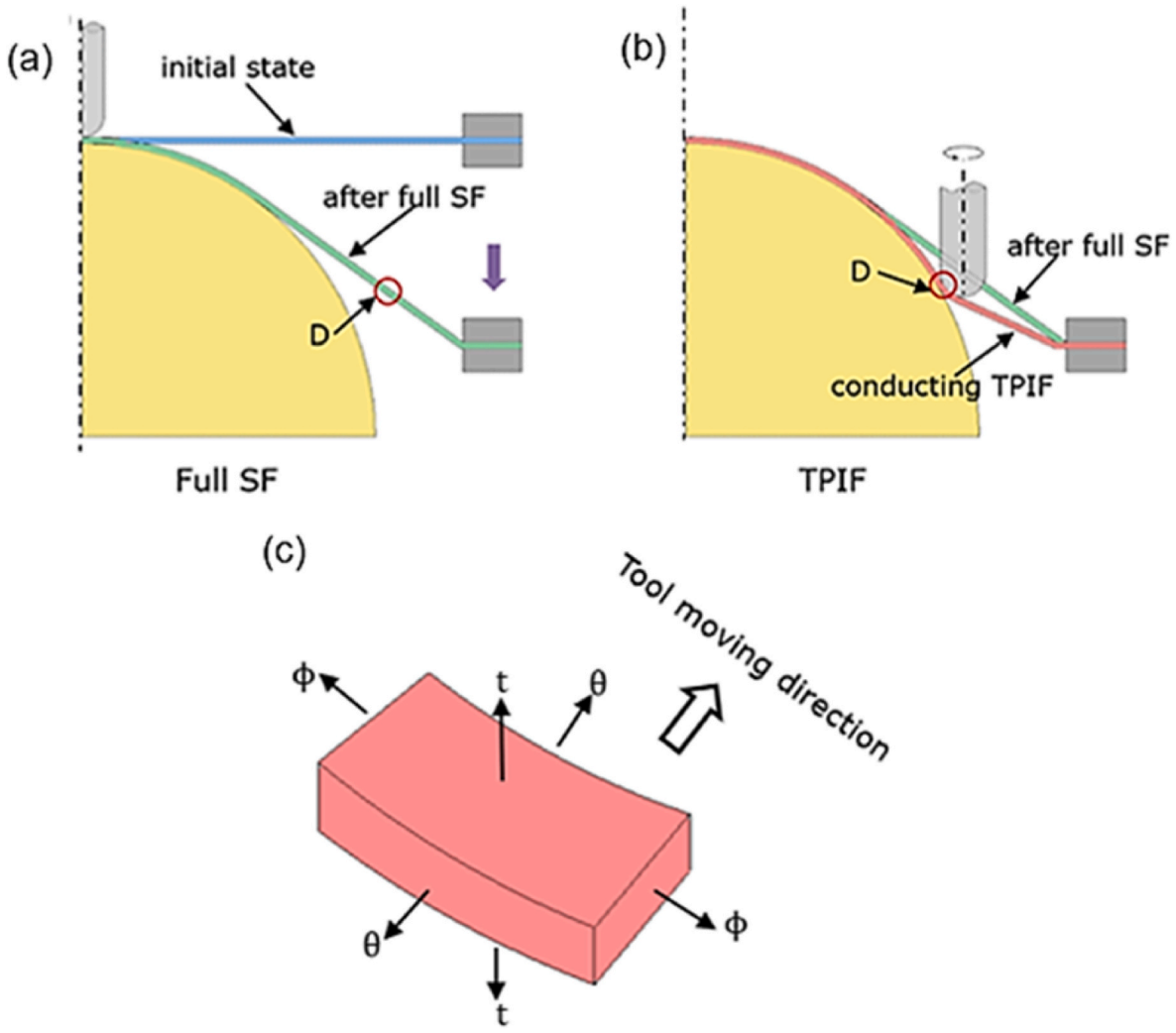

Fig. 14. Illustrations of the hybrid full stretch forming and TPIF process, (a) first stage: full stretch forming process, and (b) second stage: TPIF process; (c) schematic of the meridional (φ), circumferential (θ), and through-thickness (t) directions.

a meridional cross-section. The meridional cross-section was divided into three regions, as shown in Fig. 11. Region A represented the deformation region. Region B was the transition region, where the forming tool stopped at the end of the TPIF or DL-TPIF processes to achieve the maximum draw angle. Region C was the clamping region, which was clamped and supported by the blank holder.

5.1.1. Strain distributions and analysis

Fig. 12 shows the distributions of equivalent plastic strain (PEEQ) obtained from FE simulations. In all six forming processes, the maximum strain concentrations were presented at the largest wall angle. It was obvious from Fig. 12 (c) and (f) that the strain distributions became more uniform when combining the full stretch forming process than the processes with or without 15 mm of pre-stretching. The maximum PEEQ values decreased as the pre-stretching depth increased.

From Fig. 12 (a)–(f), the peak PEEQ values from the models involved in the TPIF processes were always greater than those with the DL-TPIF processes. One explanation could be that the target blank sheet in the DL-TPIF process was not rigidly clamped, which allowed more material in the clamping area to draw into the deformation region. Therefore, less

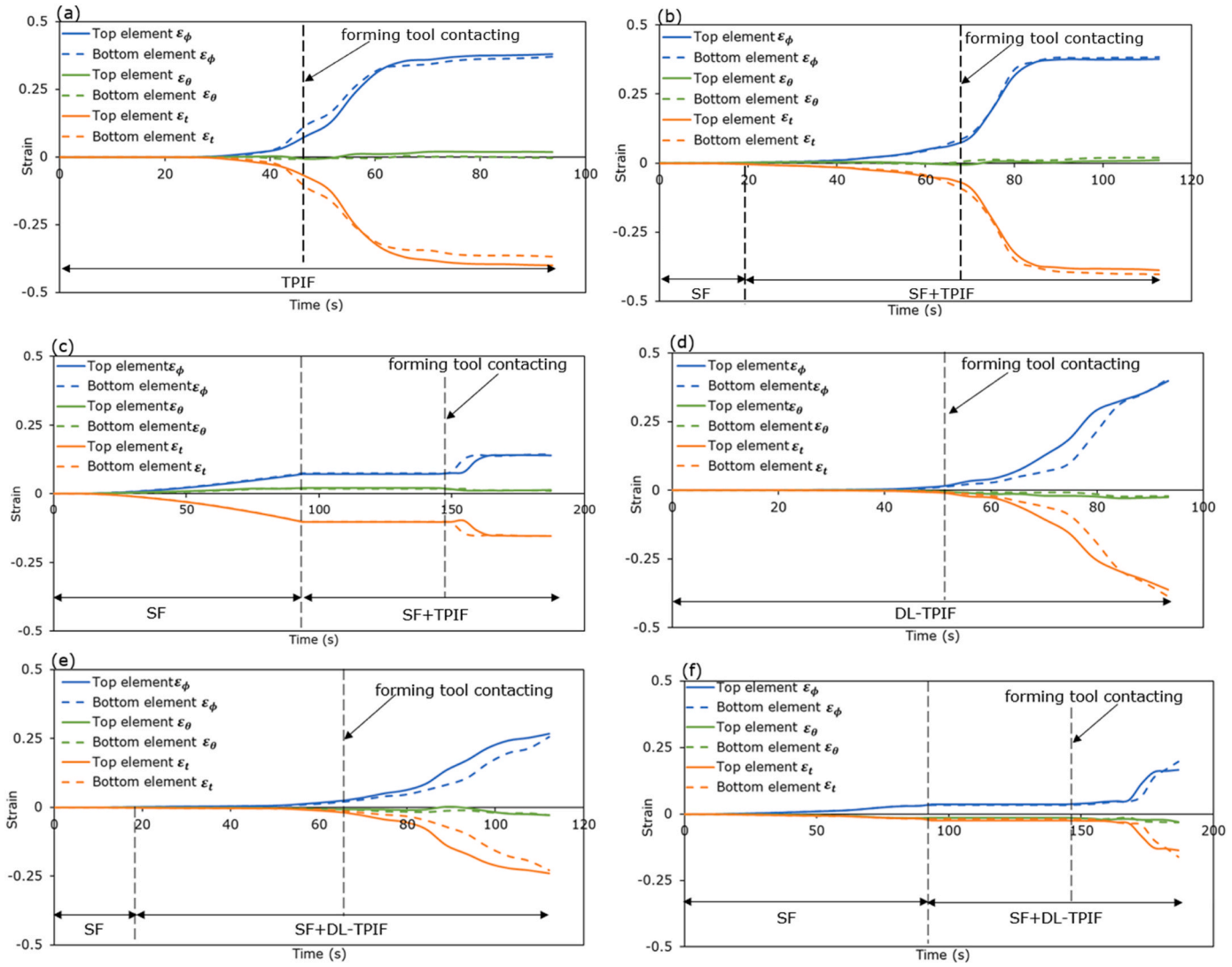

Fig. 15. Strain evaluations history along the meridional, circumferential and through-thickness directions, (a) conventional TPIF, (b) hybrid 15 mm SF + TPIF, (c) hybrid full SF + TPIF, (d) DL-TPIF, (e) hybrid 15 mm SF + DL-TPIF (f) hybrid full SF + DL-TPIF processes.

stretching could be applied to the target blank sheet, and more uniform strain distributions could be obtained as compared to the parts deformed by the TPIF process.

According to Fig. 12 (a) (b) (d) (e), when conducting a 15 mm pre-stretching and without the stretch forming process, the strain distributions started from extremely low values at the centre of the domed shape and increased progressively to reach the maximum values at the largest wall angle. When employing the full stretch forming process, relatively high strain values were generated at the centre, as shown in Fig. 12 (c) (f). These values decreased for a small area and then increased rapidly to peak values corresponding to the maximum draw angle.

Fig. 13 shows the strain distributions after the full stretch forming process. The highest strains were concentrated in the central region and tended to decrease gradually with the increased draw angle. In contrast, in the case of the TPIF and DL-TPIF processes, the strain distributions increased with the wall angle, as shown in Fig. 12 (a) and (d). These indicated that the material deformation modes in the stretch forming process and TPIF (or DL-TPIF) processes were different, and more material from the central region could be deformed by the stretch forming process instead of by either the TPIF or DL-TPIF processes. This finding was generally agreed with Araghi et al. [5] and Zhang et al. [15]. As a result, the combination of full pre-stretching and TPIF (DL-TPIF) processes has the capability to achieve a more uniform thickness distribution than the conventional TPIF or DL-TPIF processes alone.

In order to investigate the strain and stress variations in various forming processes, location D was picked from the deformation region of the dome shape to conduct the analysis, as shown in Fig. 14. In the hybrid stretch forming and TPIF process, the top of the dome profile has already been produced by the pre-stretching process, and the TPIF process was used to complete the rest of the designed shape. Location D was affected and deformed by the stretch forming and TPIF processes, so it was selected to conduct the strain and stress analysis.

Fig. 15 presents the evolutions of strain components between the top and bottom elements against the forming time. According to Fig. 14 (c), the strain along the inclined wall and perpendicular to the tool motion is defined as meridional strain ε_φ, along the tool moving direction is defined as circumferential strain ε_θ, and the through-thickness direction is defined as through-thickness strain ε_t.

From Fig. 15, in all forming processes, although the circumferential strains were close to zero, the meridional and through-thickness strains were much larger than the circumferential strain. This general trend of strain results confirmed that the material deformation mode in the ISF process was close to a typical plane strain condition in conventional ISF [23]. The results showed that the proposed hybrid stretch forming and DL-TPIF process also satisfied the plane strain condition.

It could be found that the meridional strains in the six forming

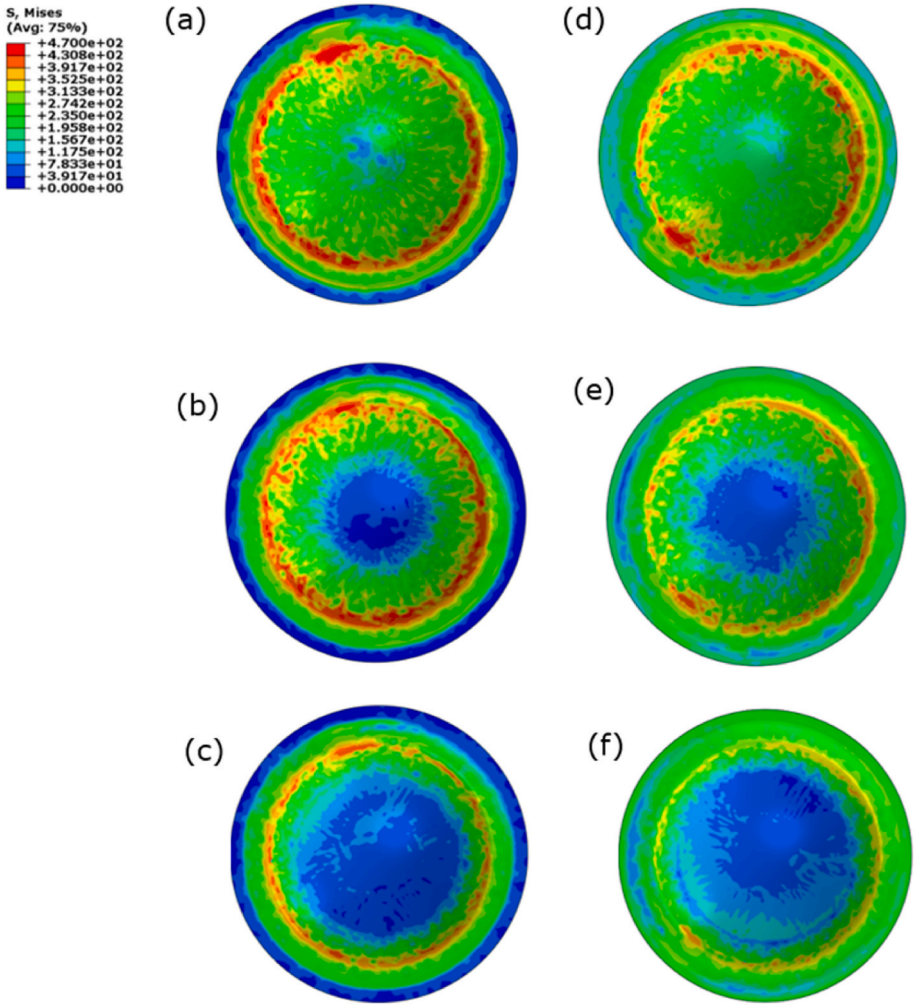

Fig. 16. von Mises stress distributions for the dome case, produced by (a) TPIF, (b) SF-15 + TPIF, (c) SF-full + TPIF, (d) DL-TPIF, (e) SF-15 + DL-TPIF, (f) SF-full + DL-TPIF processes.

processes were tensile strains, and the through-thickness strains were compressive strains from both top and bottom elements. The values of all strain components continuously increased with the forming time after contact with the forming tool, then followed by a steady stage when using the TPIF processes, as shown in Fig. 15 (a), (b), and (c). This result was in agreement with the investigation conducted by Li et al. [24]. The authors explained that the deformation of the material tended to transfer from distributed deformation to a highly localised deformation in the contact region around the forming tool. However, when using the proposed DL-TPIF process, after contacting with the forming tool, the values of all strain components kept increasing incrementally until the end of the forming operations, as presented in Fig. 15 (d), (e), and (f). It indicated that the material deformation was distributed deformation for the DL-TPIF processes. This was attributed to the arrangement of the DL-TPIF process. The target blank sheet was not physically clamped by the blank holders. Furthermore, with the increase in stretch forming depth, the amount of deformation decreased, which resulted in reductions in the value of strains along the meridional and through-thickness directions.

5.1.2. *Stress distributions and analysis*

Fig. 16 presents the von Mises stress distributions obtained from FE simulations for various forming processes. When comparing the six forming processes, the highest value of maximum stress was generated by the conventional TPIF process, and the lowest value of maximum stress was obtained by the hybrid full stretch forming and DL-TPIF process. The most uniform stress distribution was also produced by the hybrid full stretch forming and DL-TPIF process.

In each forming case, the minimum stress was concentrated in the central region, and the value of stress increased progressively to reach the maximum stress located in the largest wall angle region. It was obvious that the stress distribution became more uniform with the increase in pre-stretching depth. And the hybrid forming processes could lead to less stress than the TPIF (or DL-TPIF) processes. Moreover, under the same pre-stretching condition, the maximum stress value of the part produced by the hybrid DL-TPIF process was smaller than that produced by the hybrid TPIF process, and the stress distribution was more homogenous. This was because the target blank sheet was not rigidly clamped by the blank holders in the hybrid DL-TPIF process, and the stretching deformation applied to the blank sheet was reduced as compared to the hybrid TPIF process.

Fig. 17 shows the stress components in the local coordinate system of location D for the various forming processes. The evolutions of meridional stress (σ_φ), circumferential stress (σ_θ), and through-thickness stress (σ_t) were compared between the top and bottom elements against the forming time.

The smaller through-thickness stress σ_t difference between the top and bottom layers would result in a smaller springback after the loads were released [25]. During the hybrid forming processes, the local springback occurred simultaneously with the displacement of the forming tool, while the global springback took place when the workpiece was unclamped from the blank holders. According to Fig. 18, the

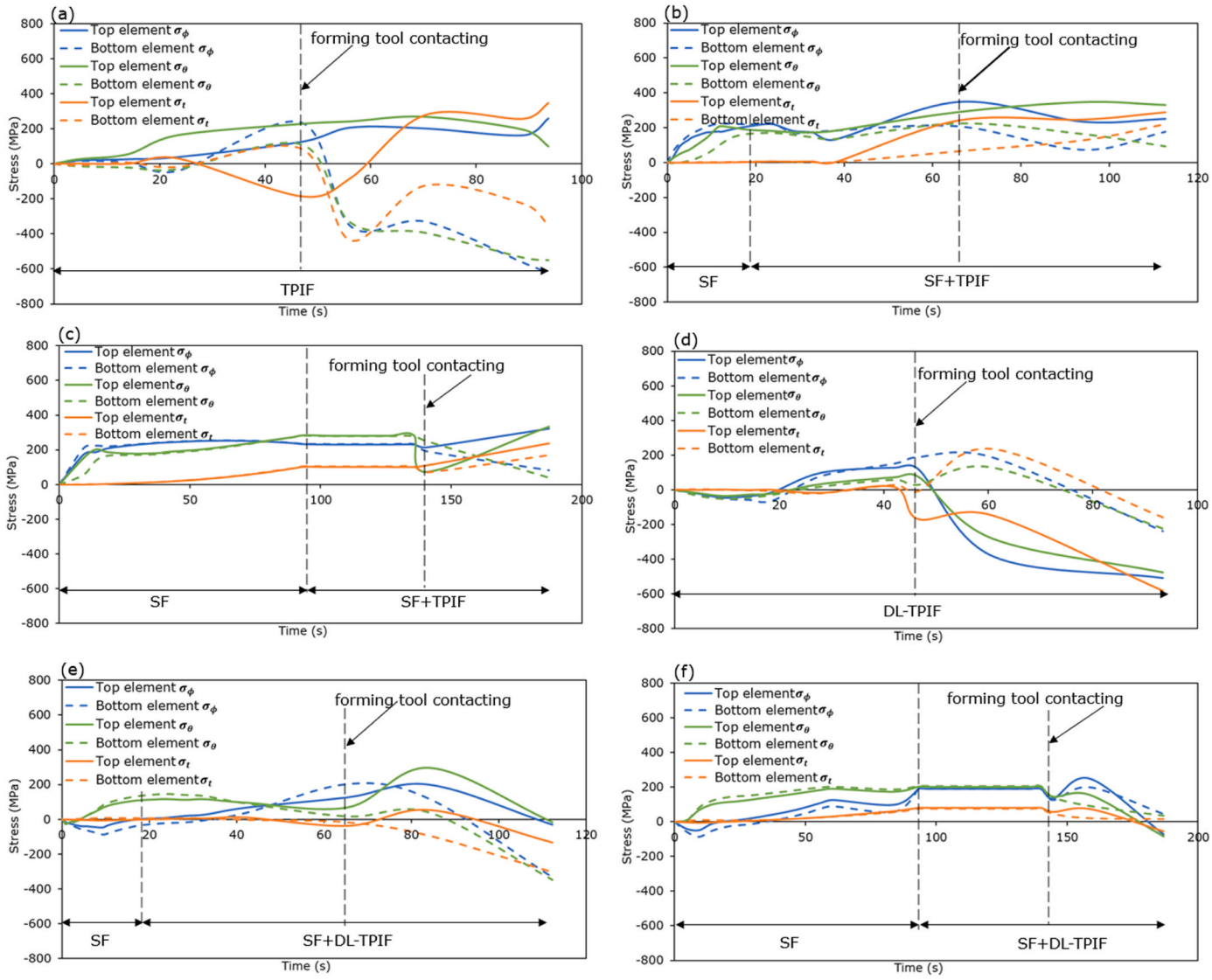

Fig. 17. Stress evaluations history along the meridional, circumferential and through thickness directions, (a) conventional TPIF, (b) hybrid 15 mm SF + TPIF, (c) hybrid full SF + TPIF, (d) DL-TPIF, (e) hybrid 15 mm SF + DL-TPIF (f) hybrid full SF + DL-TPIF processes.

largest through-thickness stress σ_t difference between the top and bottom elements was obtained by the conventional TPIF process, while the smallest stress difference was achieved by the hybrid full stretch forming and DL-TPIF process. Therefore, these results indicated that the proposed hybrid stretch forming and DL-TPIF process would be more like to reduce the amount of springback and result in better geometrical accuracy as compared to the conventional TPIF process.

In Fig. 17 (a), when the forming tool was in location D, the through-thickness stress σ_t in the conventional TPIF process deformed part was compressive-to-tensile from the top to the bottom element. In the hybrid stretch forming and TPIF process, the through-thickness stress σ_t was tensile-to-tensile, as presented in Fig. 17 (b) and (c). This was due to the fact that the tensile stress was applied to the blank sheet during the first step of the pre-stretching operation. The top and bottom elements were both under stretching before the tool contact. The meridional stress σ_φ, circumferential stress σ_θ, and through-thickness stress σ_t were all tensile stresses. When the forming tool moved to location D, the compressive stress from the tool was smaller than the tensile stress. Therefore, both top and bottom elements were under tension, which might lead to less local springback after the tool left location D as compared to the conventional TPIF process.

Similar findings were observed in the DL-TPIF and hybrid full stretch forming and DL-TPIF processes. However, when the forming tool moved to location D in the hybrid 15 mm stretch forming and DL-TPIF process, the through-thickness stress σ_t was compressive-to-compressive from the top to the bottom element, as shown in Fig. 17 (e). Chang et al. [17] compared the through-thickness stress between the conventional ISF and three-layer ISF processes, the results showed that, due to the extra compressive stress of the target blank sheet on the upper dummy sheet in the three-layer ISF process, the through-thickness stress σ_t in tool contact region was obviously larger than that in the conventional ISF process. Although 15 mm of the stretch forming process was conducted, the tensile stress induced on the target blank sheet was not large enough. In addition, the upper dummy sheet could provide extra compressive stress. Hence, the top element was under compression in the thickness direction when combining the 15 mm pre-stretching and DL-TPIF processes.

In the hybrid stretch forming and DL-TPIF process, the top and bottom elements along the meridional direction were under compression and tended to be in tension with the increase in forming time during the first pre-stretching operation. In the hybrid stretch forming and TPIF process, the top and bottom elements along the three directions were under stretching before the forming tool was in contact with the upper dummy sheet. The meridional stress σ_φ, circumferential stress σ_θ, and

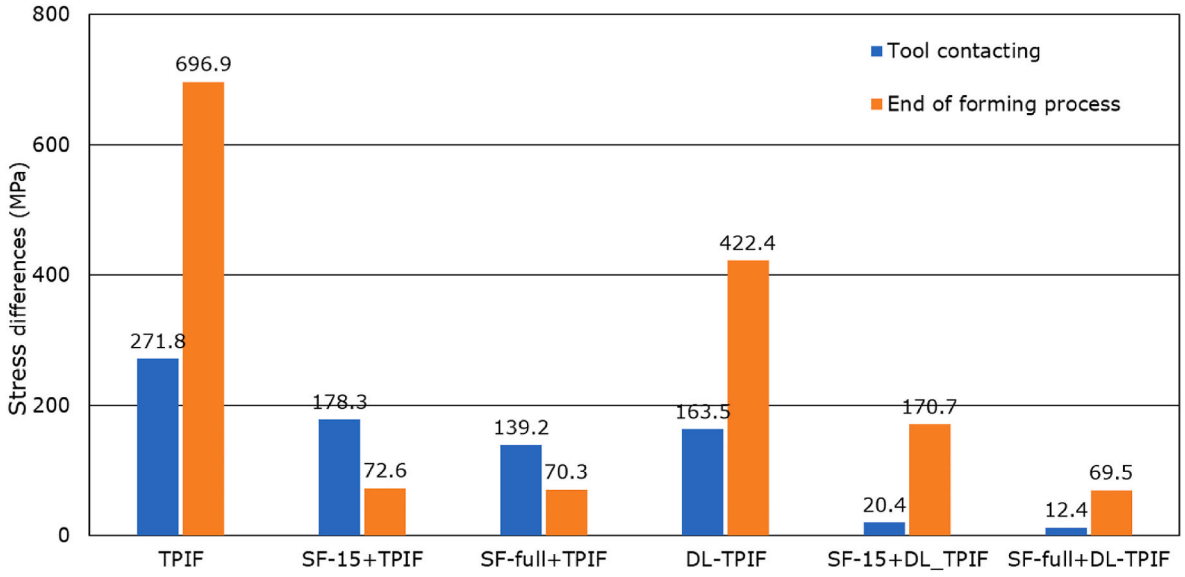

Fig. 18. Through thickness stress differences between the top and bottom elements.

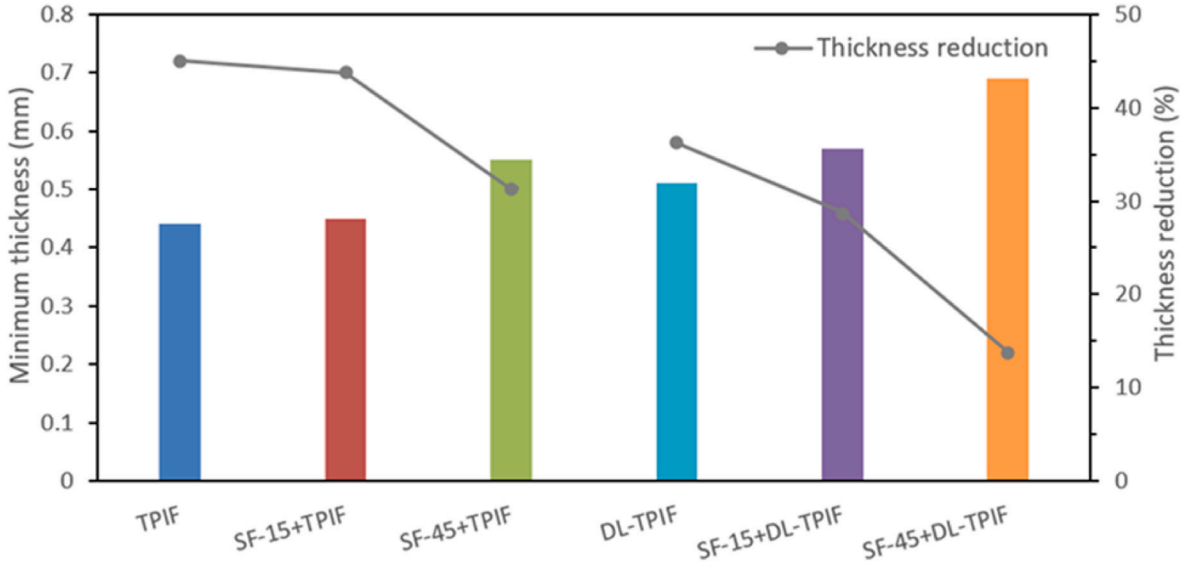

Fig. 19. Comparisons of the minimum thickness and the trend of thickness reduction from six forming processes for the dome shape.

through-thickness stress σ_t of top and bottom elements were tensile-to-tensile during the second stage of the hybrid stretch forming and TPIF process. For the hybrid stretch forming and DL-TPIF process, the stresses were compressive-to-compressive or compressive-to-tensile from top to bottom elements. These were attributed to the arrangement of the DL-TPIF process. The extra compressive stress could be provided by the upper dummy sheet. As the target blank sheet in the DL-TPIF process was not rigidly clamped, this resulted in less stretching being applied to the sheet.

In summary, in the hybrid forming processes, the first stage of pre-stretching operation induces tension in the blank sheet and affects the stress distributions in the second stage of TPIF (or DL-TPIF) process, which leads to a reduced stress difference between the top and bottom elements. In the DL-TPIF process, extra compressive stress was applied to the target blank sheet due to the use of an upper dummy sheet. Additionally, the target blank sheet was not rigidly clamped, so less stretching was applied to the sheet as compared to the TPIF process.

5.1.3. Thickness variations

The minimum thickness for each forming process was compared in Fig. 19. The maximum thickness reduction of the parts produced by the DL-TPIF process was clearly smaller than that obtained from the TPIF process, with or without pre-stretching. The initial thickness of the blank sheet was 0.8 mm. In the hybrid full pre-stretching and DL-TPIF process, the minimum thickness was only 0.69 mm, which was equivalent to a thickness reduction of 13.8%. This value was less than 1/3 of the thickness reduction in the part deformed by the conventional TPIF process (45%).

Fig. 20 presents the comparisons of the thickness distributions along the meridional cross-section obtained from experimental testing and FE simulations. Due to the capacity of the lifting machine, a full stretch forming process could not be conducted. Fig. 20 (c) only compares the FE results between the hybrid stretch forming and TPIF process and the hybrid stretch forming and DL-TPIF process. To show the results intuitively, the six forming processes were divided into three groups according to the pre-stretching depth condition. The FE predicted results

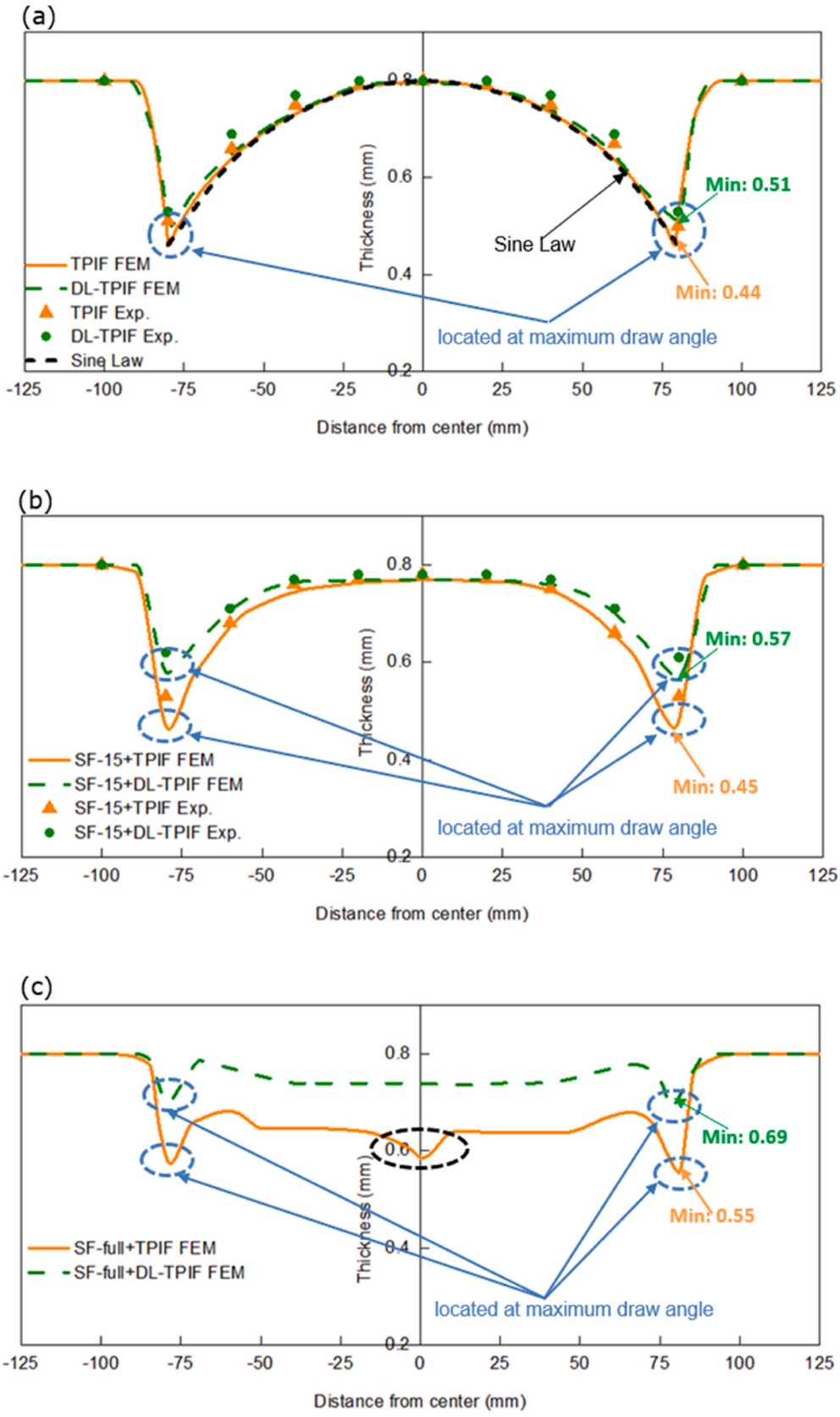

Fig. 20. Comparisons of thickness distributions obtained from: (a) TPIF vs DL-TPIF, (b) SF-15+TPIF vs SF-15+DL-TPIF, (c) SF-full + TPIF vs SF-full + DL-TPIF process.

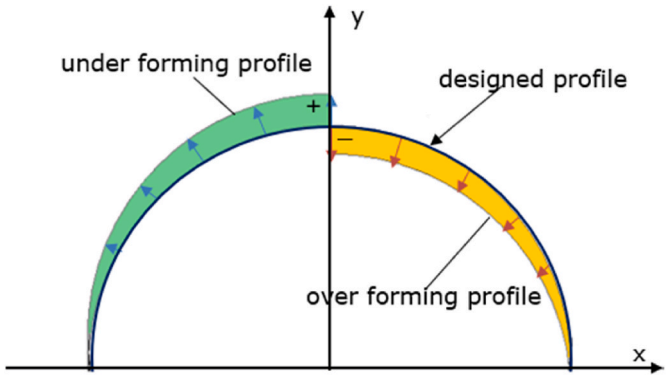

Fig. 21. Illustrations of the under forming and over forming profiles.

were in agreement with the measured results. Tendencies of thickness distributions within each group were similar.

In all six forming processes, the wall thickness decreased along the radius direction until the largest wall angle, where the maximum thinning occurred. This was in good correlation with the strain distribution results, as presented in Fig. 12. In comparisons within all six forming processes, the most uniform thickness distribution was found in the part produced by the hybrid full stretch forming and DL-TPIF process.

As shown in Fig. 20 (a), when conducting the TPIF or DL-TPIF processes, the sheet thickness decreased in the radial direction with increasing wall angle, which was in accordance with the Sine law. In the case of 15 mm pre-stretching, the sheet thickness kept stable in a small region at the centre and decreased gradually. Less thinning was found in the largest wall angle as compared to the parts produced by the TPIF or DL-TPIF processes without pre-stretching. In the hybrid full stretch forming and TPIF (or DL-TPIF) process, the thickness in the deformation region was almost distributed homogeneously and then dropped to small values at the location of the largest wall angle, as shown in Fig. 20 (c). However, in the hybrid stretch forming and TPIF process, in the highlighted region, the thickness variation was not as uniform as the results from the hybrid full stretch forming and DL-TPIF process. It can be concluded that the stretch forming process can be used to induce thinning in regions that would not be deformed by the TPIF and DL-TPIF processes, and increasing the amount of pre-stretching depth would result in more homogenous thickness distributions.

As shown in Fig. 20, the thickness distributions between the TPIF and DL-TPIF processes under the same pre-stretching condition were similar. However, the thickness reduction of the parts produced by the DL-TPIF process was smaller than that of the TPIF process. For example, when combining the full pre-stretching process, the maximum thickness reduction in the DL-TPIF process was 13.8% and 28.8% for the TPIF process. This can be explained by the arrangement of the proposed DL-TPIF process. The target blank sheet in the DL-TPIF process was not rigidly clamped, so more material from the clamping area flowed into the deformation region. As a result, the thickness reduction in the case of the DL-TPIF was smaller than that in the TPIF process to achieve a uniform thickness distribution. When combined with the stretch forming process, these effects became more pronounced as the pre-stretching depth increased.

5.1.4. Geometrical accuracy

In this study, the dimensional errors were used to quantify the geometrical inaccuracies, which were obtained by comparing the deviations between the designed CAD model and FE predicted results. The negative dimensional errors represent the over-forming, while the positive dimensional errors indicate the under-forming, as shown in Fig. 21.

Fig. 22 shows the dimensional errors of the deformed parts before and after unclamping from the blank holders. In all cases, the maximum dimensional errors were observed in the largest draw-angle region. And the geometrical inaccuracies increased after the parts were unclamped from the blank holders, which could be explained by the global springback. In the ISF process, there were three common types of springback. The first was the local springback, which occurred simultaneously with the displacement of the forming tool. The second was the global springback, which took place after the forming tool was removed and the workpiece was unclamped from the blank holders. The last was caused by the trimming operation, which was due to residual stress redistribution and hence increased geometrical deviations [18,26]. Further optimisation of toolpath strategies, die development, and ISF specific compensation methods can be considered to reduce the degree of springback [27,28]. In comparisons among the six different cases, the maximum global springback was obtained from the part produced by the conventional TPIF process. On the other hand, the minimum value was observed in the hybrid stretch forming and DL-TPIF process produced part.

The geometrical accuracy could be improved with an increase in pre-stretching depth, as shown in Fig. 23. This finding generally agreed with the results from Araghi et al. [5,12]. The authors mentioned that applying stretch forming simultaneously to the TPIF process could minimise the residual stresses caused by the cyclic bending and unbending, which reduced unwanted deviations. Pohlak et al. [29] also stated that increasing stretching force could enhance geometrical accuracy because the pre-stretching operation could induce extra tension in the material. The applied tension could reduce the differential stress to address the springback effect. From Fig. 17 (a), in the conventional TPIF process, the stress state through thickness was tensile-to-compressive from the top to the bottom element. When the part was unloaded, either from the forming tool or blank holders, the difference between tensile stress and compressive stress would change the accuracy. When combining the stretch forming process, the stress difference between the top and bottom elements through-thickness direction became smaller. As a result, it can be concluded that the pre-stretching reduced deviations caused by the springback. In the new variant of the hybrid forming process, a more precise part can be obtained by increasing stretch forming depth.

Fig. 23 compares the maximum dimensional errors between the FE predicted and experimental testing results. The maximum difference was around 0.5 mm. This discrepancy could be explained by the inaccurate prediction of material springback, and the implemented material behaviour was not strictly identical to the real situation in the FE analysis.

By evaluating the proposed DL-TPIF process, the overall geometrical accuracy of the part produced by the hybrid stretch forming and DL-TPIF process was better than that of the hybrid stretch forming and TPIF process under the same pre-stretching condition. This was due to the fact that the upper dummy sheet provided extra constraints to the target blank sheet, which minimised the influence of the local springback during the forming operation.

5.2. Case 2: irregular shape

In the second case study, an irregular shape was employed as the designed geometry, as shown in Fig. 4 (b). The largest draw angle of this asymmetrical profile was around 70°. Fig. 24 presents the tested deformed irregular parts produced by the hybrid stretch forming and TPIF, and hybrid stretch forming and DL-TPIF processes under different pre-stretching conditions.

The experimental measured and FE simulation results were presented along the longitudinal direction (A-A cross-section) and vertical direction (B–B cross-section), as shown in Fig. 6 (b). The A-A cross-section of the designed irregular profile was divided into three regions, which followed the region division guideline in Fig. 25. Regions A, B, and C represent the deformation region, the transition region, and the clamping region, respectively.

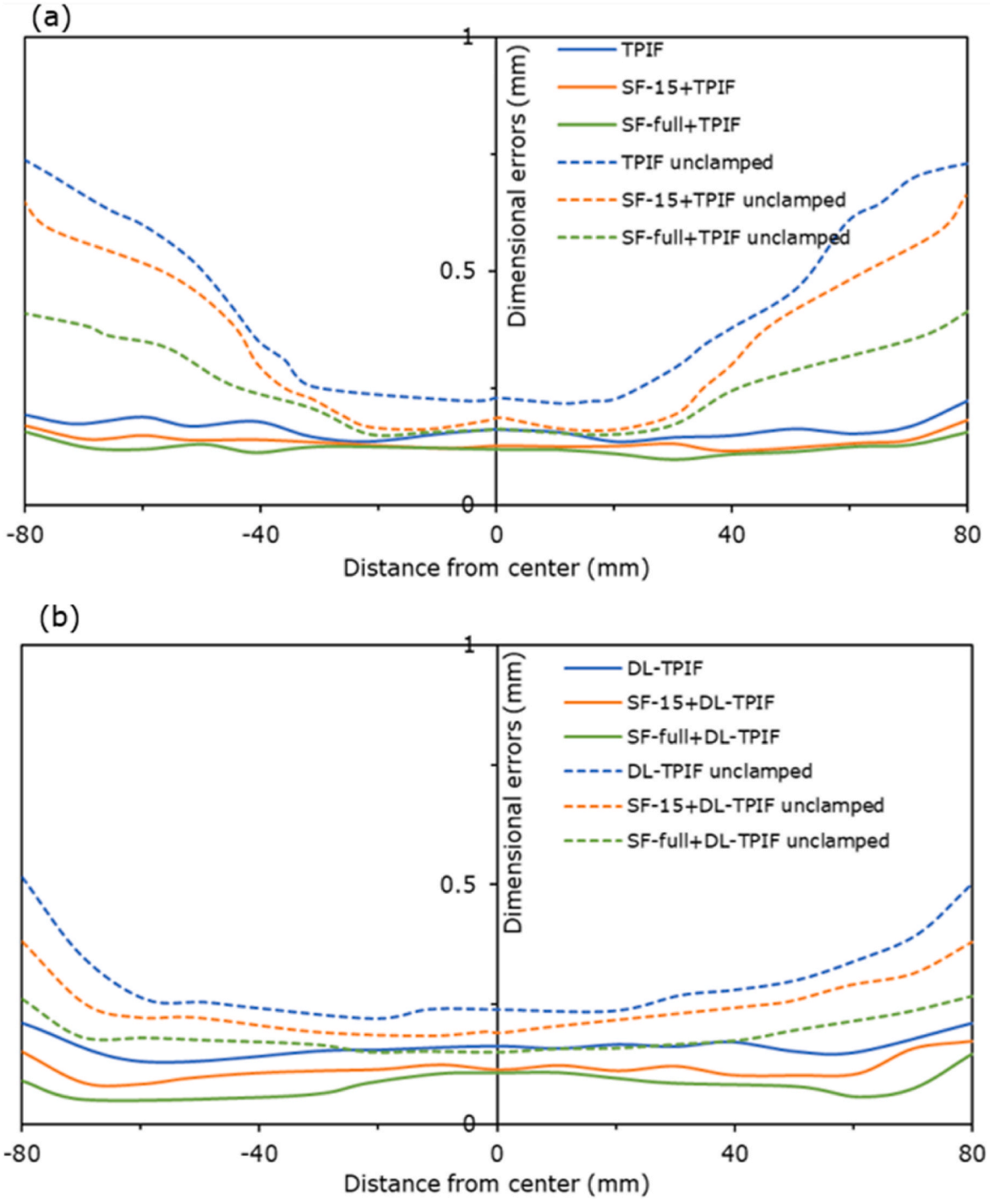

Fig. 22. The dimensional errors of the parts before and after unclamping from the blank holders (a) the hybrid SF and TPIF process, and (b) the hybrid SF and DL-TPIF process with different pre-stretching conditions.

5.2.1. Strain and stress distributions

Fig. 26 shows the distributions of equivalent plastic strain for the hybrid stretch forming and TPIF process, and the hybrid stretch forming and DL-TPIF process under different pre-stretching conditions, as listed in Table 1. Compared to the dome shape, the maximum wall angle of this irregular profile increased from 57° to 70°, and the differences in PEEQ values among the six forming processes increased notably. According to Fig. 26, the most homogeneous strain distributions were obtained by the hybrid full stretch forming and DL-TPIF process, and the maximum PEEQ value was the smallest, which was almost 1/5 of the conventional TPIF process.

Large strain concentrations occurred in the transition region (region B) for the TPIF, SF-15+TPIF, DL-TPIF, and SF-15+DL-TPIF processes. In these four forming processes, the PEEQ values increased with the increase in draw angles. However, large strains occurred in the deformation and transition regions when combining the full pre-stretching with TPIF or DL-TPIF processes. In the deformation region, the maximum strain was observed around 30 mm from the B–B axis. This was because the designed irregular profile was asymmetrical, and the draw angle on the right side was larger than that of the left side. When conducting the full stretch forming as a pre-forming step, the majority of the part was deformed by the stretch forming process. The material deformations

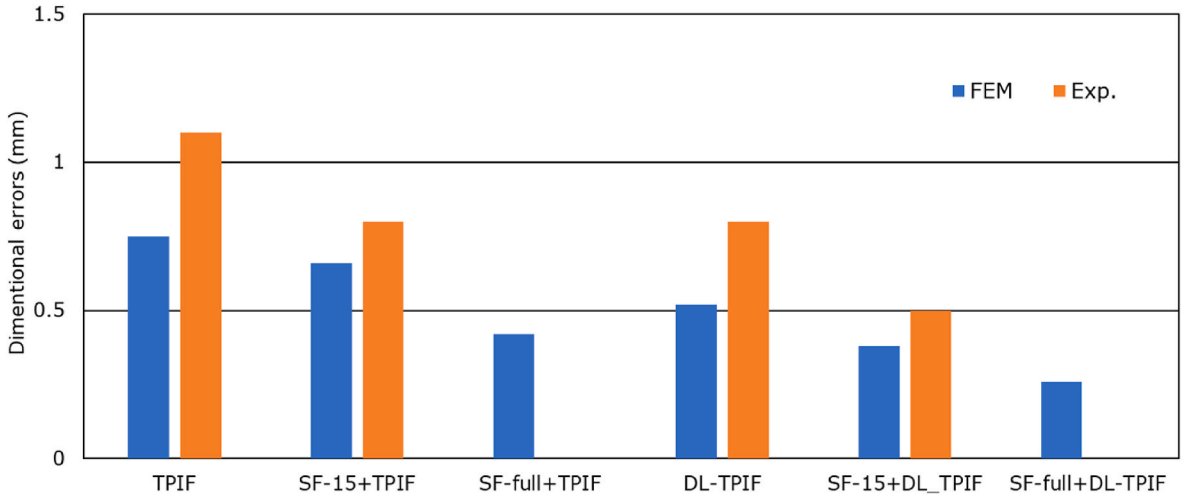

Fig. 23. Comparisons of the maximum dimensional errors between the FE predicted and experimental testing results for the dome shape.

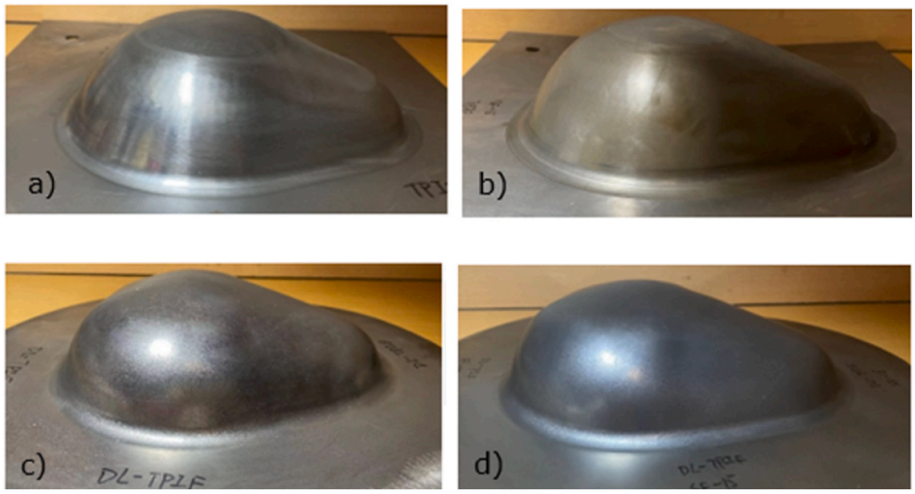

Fig. 24. Experimental testing results obtained from (a) conventional TPIF, (b) SF-15+TPIF, (c) DL-TPIF, and (d) SF-15+DL-TPIF processes.

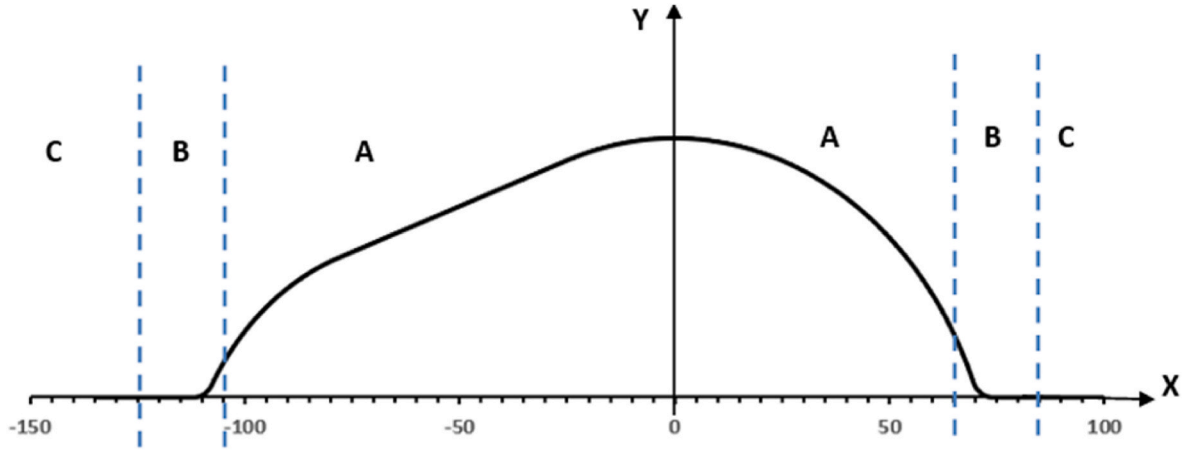

Fig. 25. A–A cross section along the longitudinal direction for measurements and a schematic of region divisions for the irregular shape.

caused by the stretch forming and TPIF (or DL-TPIF) processes were different. As a result, the strain distributions of the hybrid full stretch forming and TPIF (or DL-TPIF) processes were different from the other four forming processes.

The maximum PEEQ values of the parts produced by the TPIF process were always larger than those produced by the DL-TPIF process. At the same time, the maximum PEEQ values decreased with the increase in the pre-stretching depth. These indicated that the proposed hybrid stretch

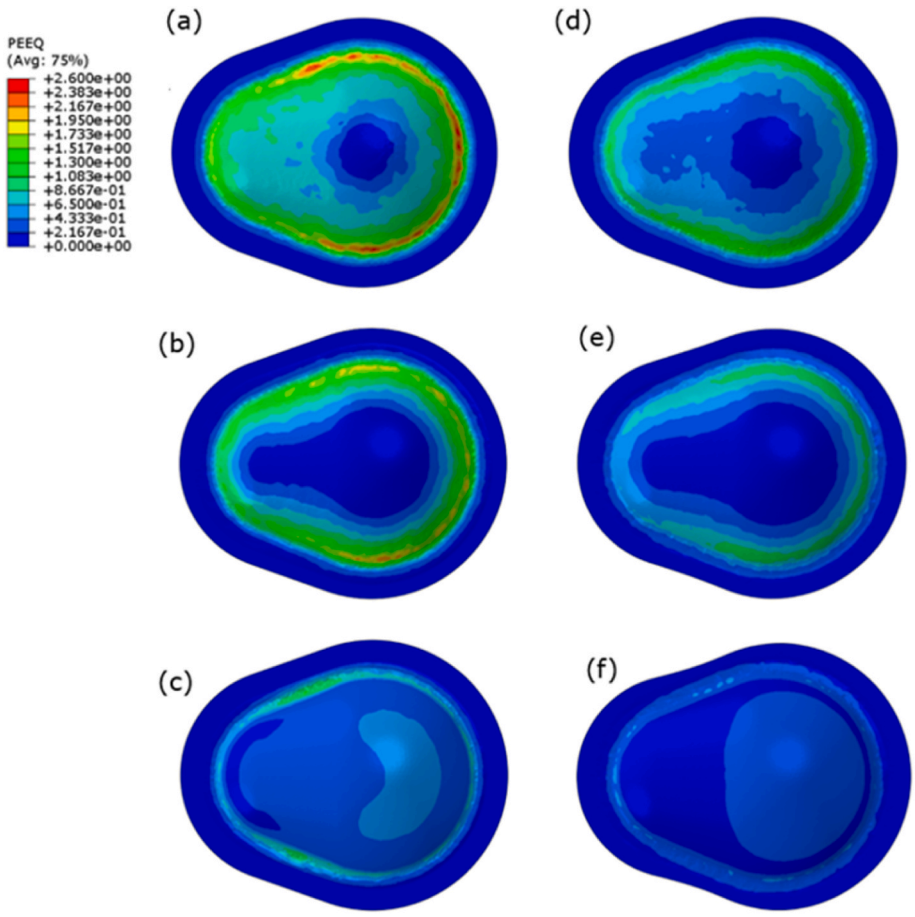

Fig. 26. Equivalent plastic strain distributions obtained from FE simulation produced by (a) TPIF, (b) SF-15 + TPIF, (c) SF-full + TPIF, (d) DL-TPIF, (e) SF-15 + DL-TPIF, (f) SF-full + DL-TPIF processes.

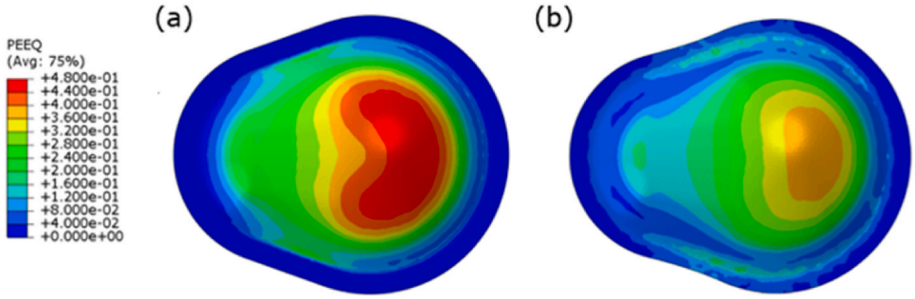

Fig. 27. Equivalent plastic strain distributions after full pre-stretching (a) TPIF, and (b) DL-TPIF processes.

forming and DL-TPIF process could result in a more uniform strain distribution than the conventional TPIF process. This effect became more pronounced as the pre-stretching depth was increased.

Fig. 27 compares the PEEQ distributions between the TPIF and DL-TPIF processes after the full pre-stretching process. In these two forming processes, the maximum PEEQ values were both concentrated at the top of the irregular shape. A higher PEEQ value was obtained from the TPIF process.

Fig. 28 presents the PEEQ distributions of the parts produced by the TPIF, DL-TPIF, and stretch forming processes to a forming depth of 15 mm. It could be found that the strain distribution of the TPIF process was identical to that of the DL-TPIF process but was different from the stretch forming process. In the case of the TPIF and DL-TPIF processes, the PEEQ values increased with the increase in draw angle, while the maximum PEEQ value was concentrated in the centre and decreased along the radius direction for the stretch forming process. These observations can be used to explain the deformation regions in the stretch forming and TPIF (or DL-TPIF) processes that were different. The stretch forming process can be employed to induce thinning in regions that would not be deformed by the TPIF and DLTPIF processes. Therefore, the hybrid stretch forming and TPIF (or DL-TPIF) can provide the possibility of achieving a more uniform thickness distribution than that obtained by either process alone.

Fig. 29 presents the von Mises stress distributions for the case of an irregular shape, obtained from the FE simulations. The maximum stress was concentrated in the region with the largest draw angle for each model. The highest stress value was generated by the conventional TPIF process. With the increase in pre-stretching depth, the amount of stress was reduced and became more uniform in the deformation region. This could be attributed to the fact that the amounts of stress induced by the

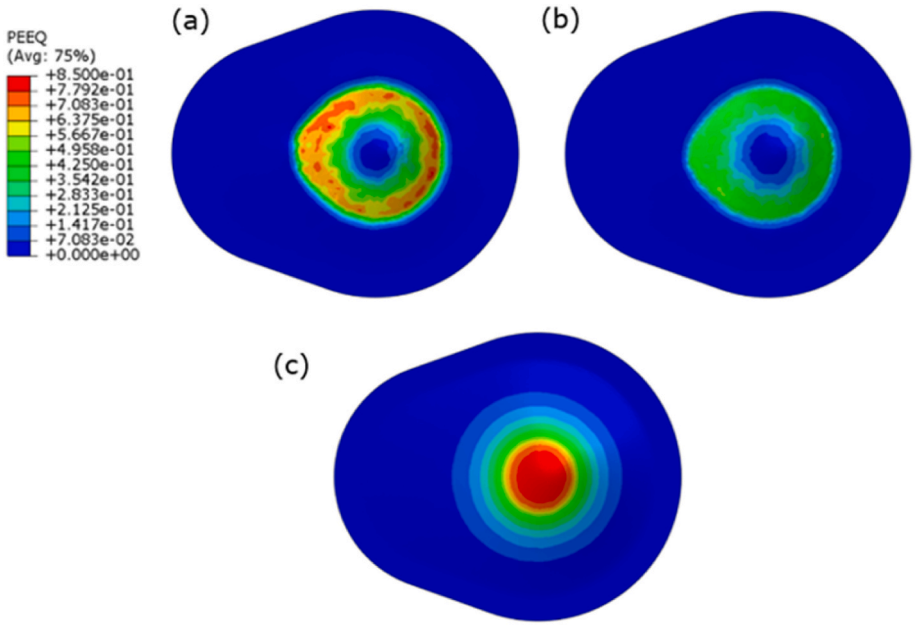

Fig. 28. Equivalent plastic strain distributions of the processes with 15 mm forming depth (a) conventional TPIF, (b) DL-TPIF, and (c) SF processes.

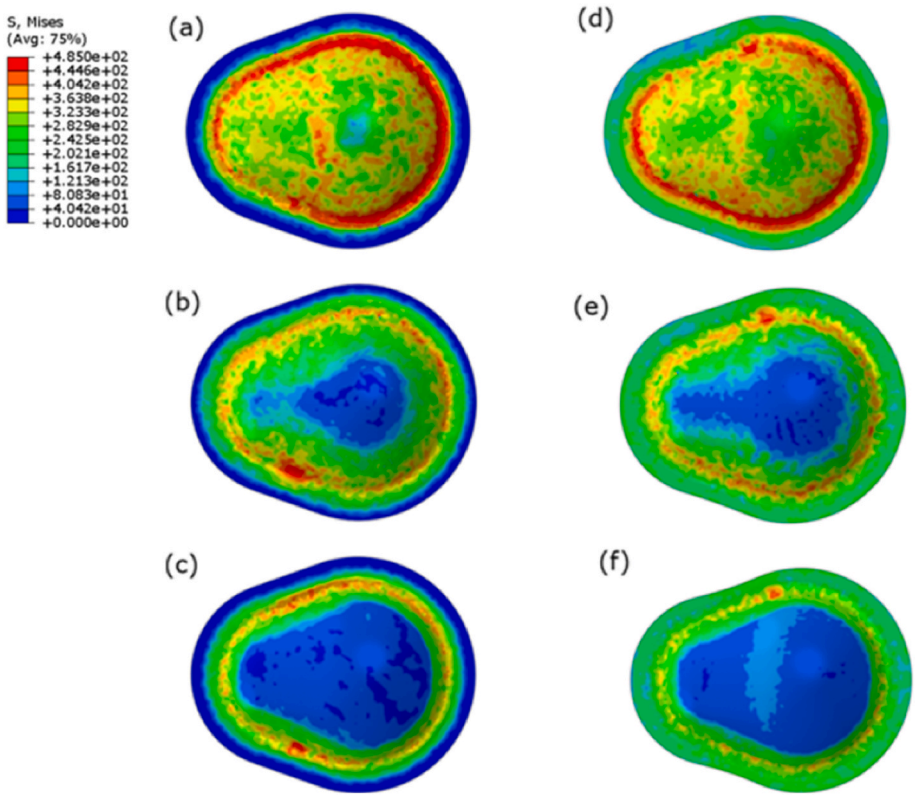

Fig. 29. Von Mises stress distributions for the irregular case, obtained from FE simulations produced by (a) TPIF, (b) SF-15 + TPIF, (c) SF-full + TPIF, (d) DL-TPIF, (e) SF-15 + DL-TPIF, (f) SF-full + DL-TPIF processes.

TPIF (or DL-TPIF) and hybrid forming processes were different. The hybrid forming could result in less amount of stress. In addition, the stress value was reduced and became more homogenous when using the DL-TPIF process to replace the TPIF process. It was due to the arrangement of the DL-TPIF process, in which less stretching was applied to the target blank sheet to allow the material in the clamping area to be drawn into the deformation during the forming operation.

5.2.2. Thickness variations

Fig. 30 shows the comparisons of the minimum thickness and thickness reduction along the longitudinal direction of all six FE models. The initial thickness of the blank sheet was 0.8 mm. Increasing the pre-stretching depth would result in a noticeable improvement in thickness reduction. The minimum thickness of the model obtained from the hybrid full stretch forming and DL-TPIF process was 0.54 mm, while the

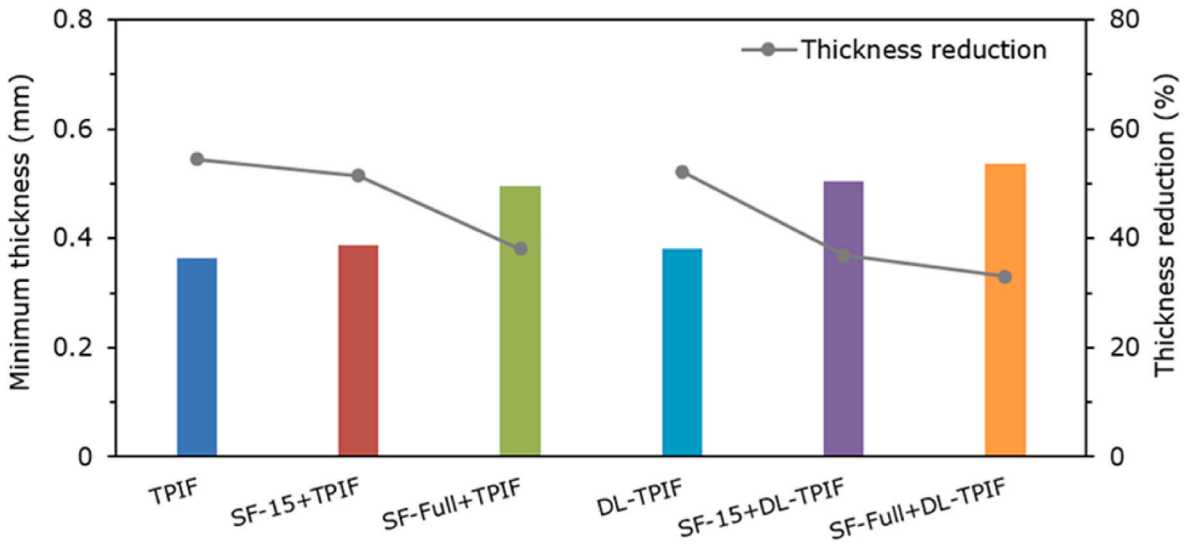

Fig. 30. Comparisons of the minimum thickness and thickness reduction along longitudinal direction among six FE forming processes for the irregular shape.

minimum thickness for the conventional TPIF process formed part was 0.36 mm. Therefore, in the proposed hybrid stretch forming and DL-TPIF process, the combined effect of the full pre-stretching and arrangement of the DL-TPIF process led to a significant reduction in sheet thinning as compared to all the other forming processes, as presented in Fig. 30.

Fig. 31 presents the comparisons of FE simulation and experimental testing results of the wall thickness distributions along the longitudinal direction. The results were divided into three groups, and each group compared the results between the TPIF and DL-TPIF processes with the same pre-stretching condition. When employing full pre-stretching, the minimum thickness occurred in the deformation region, which was 30 mm from the B–B axis. The maximum thinning was found for the other four forming processes in the transition region, and less thinning was observed at the centre of the irregular profile. The wall thickness results correlate well with the equivalent plastic strain distributions, as shown in Fig. 26. In comparing the results from the six forming processes, the most uniform thickness distribution with the least amount of sheet thinning was produced by the hybrid full stretch forming and DL-TPIF process.

The experimental results showed good agreement with the predicted thickness distributions. The overall tendencies of thickness variations between the TPIF and DL-TPIF processes under the same pre-stretching condition were similar. The minimum thickness reduction of the part produced by the hybrid stretch forming and DL-TPIF process was always smaller than that of the hybrid stretch forming and TPIF process. These indicated that the implementation of the proposed DL-TPIF process could improve sheet thinning, but the material deformation mode remained the same.

Araghi et al. [5] and Zhang et al. [15] have stated that the maximum sheet thinning in the stretch forming process was found at a certain distance from the central axis, while the minimum thickness was found at the largest draw angle for the ISF forming process to produce a dome shape. As shown in Fig. 31 (a) (b) (c), the central region thickness decreased as the pre-stretching depth increased. This was sufficient to show the different thinning behaviour between the stretch forming and TPIF (or DL-TPIF) processes. The stretch forming process could induce sheet thinning in the regions that would not be deformed by the TPIF or DL-TPIF processes. Therefore, the combination of the stretch forming and TPIF (or DL-TPIF) processes offered the possibility of achieving a more uniform thickness distribution than the stretch forming, TPIF, or DL-TPIF processes.

5.2.3. *Geometrical accuracy*

In order to compare the geometrical accuracy of the deformed parts, the results were measured in the longitudinal direction. Fig. 32 shows the dimensional errors of the parts before and after being released from the blank holders. In all cases, significant springback could be observed after unclamping. At the same time, the maximum geometrical inaccuracies were all found at the largest draw angle region.

The negative dimensional errors were observed before the workpiece was unclamped from the blank holders. And these negative dimensional errors always occurred in the large thickness reduction regions. One possible reason was that the upper surfaces of the deformed parts were picked to conduct the measurements. If the amount of sheet thinning was larger than the local springback, the dimensional errors turned negative.

The maximum dimensional errors between the predicted and measured results are compared in Fig. 33. The geometrical accuracy was improved by combining the stretch forming process. In the hybrid full stretch forming and TPIF process, the predicted maximum dimensional deviation was 0.46 mm, which was around two-thirds of the maximum dimensional error in the conventional TPIF process. And when combining the full pre-stretching with the DL-TPI process, the predicted maximum dimensional error was reduced from 0.42 mm to 0.26 mm. These could be explained by the extra tensile stress induced in the blank sheet in the first pre-stretching operation, which changed the stress distribution to reduce the degree of springback. Therefore, a more accurate part can be obtained with the increased pre-stretching depth.

Moreover, due to the use of an upper dummy sheet, the overall geometrical accuracy of the parts produced by the DL-TPIF processes was clearly higher than that of the parts deformed by the TPIF process. For example, the tested maximum dimensional error was 0.8 mm in the proposed DL-TPIF process and 1.3 mm in the conventional TPIF process. It could be explained by the fact that the upper dummy sheet provided extra constraints to the target blank sheet during the forming process to achieve a reduced amount of springback and, hence, improved geometrical accuracy as compared to the conventional TPIF process.

6. Conclusions

In this research, the proposed hybrid stretch forming and DL-TPIF process has been demonstrated by two case studies. Three stretching conditions (i.e., 0 mm, 15 mm, and full depth) were examined to evaluate the effect of pre-stretching. In order to investigate the new arrangement of the double-layer blank sheets, the parts produced by the

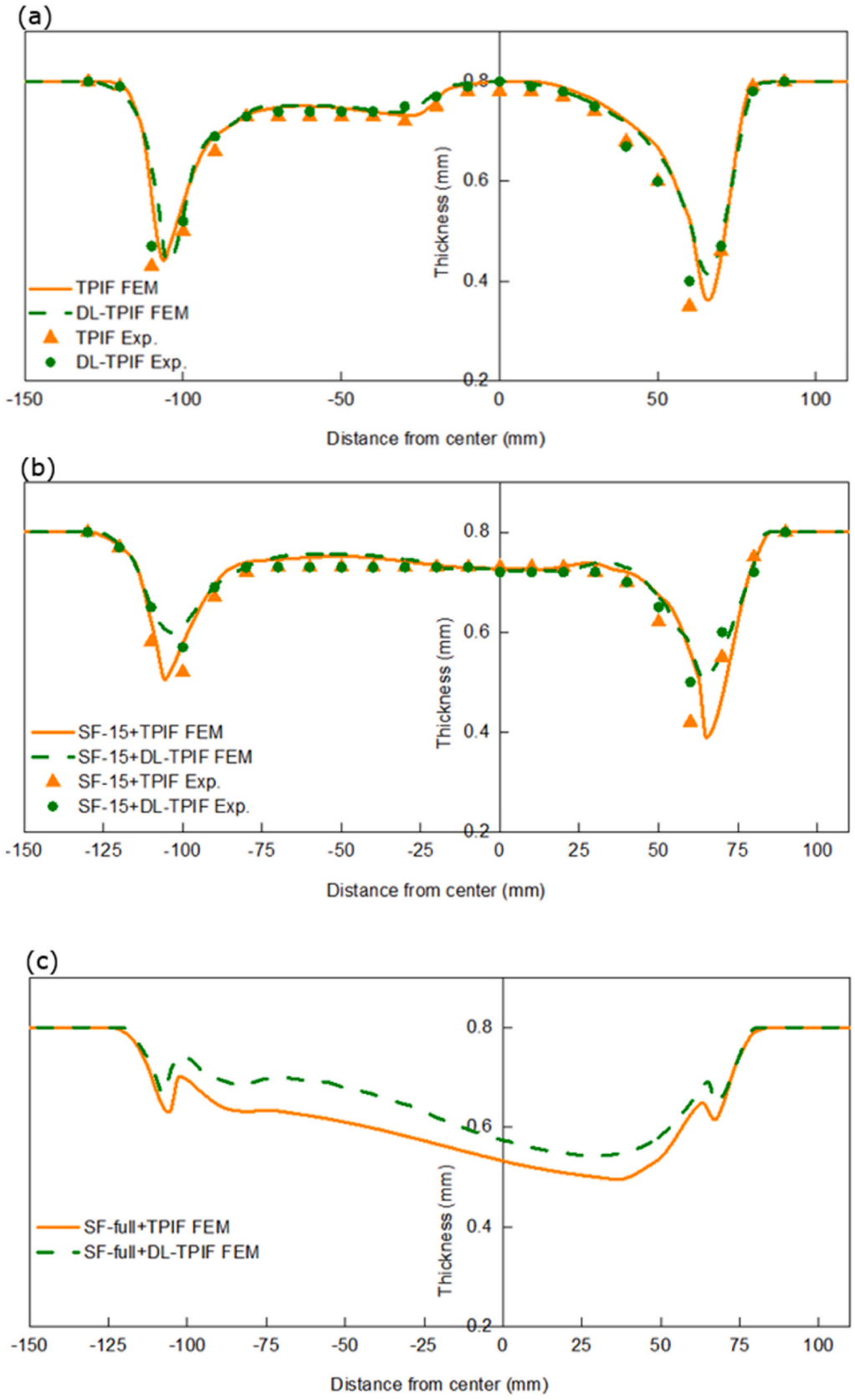

Fig. 31. Comparisons of wall thickness distribution along longitudinal direction: (a) TPIF vs DL-TPIF, (b) SF-15+TPIF vs SF-15+DL-TPIF, (c) SF-full + TPIF vs SF-full + DL-TPIF process.

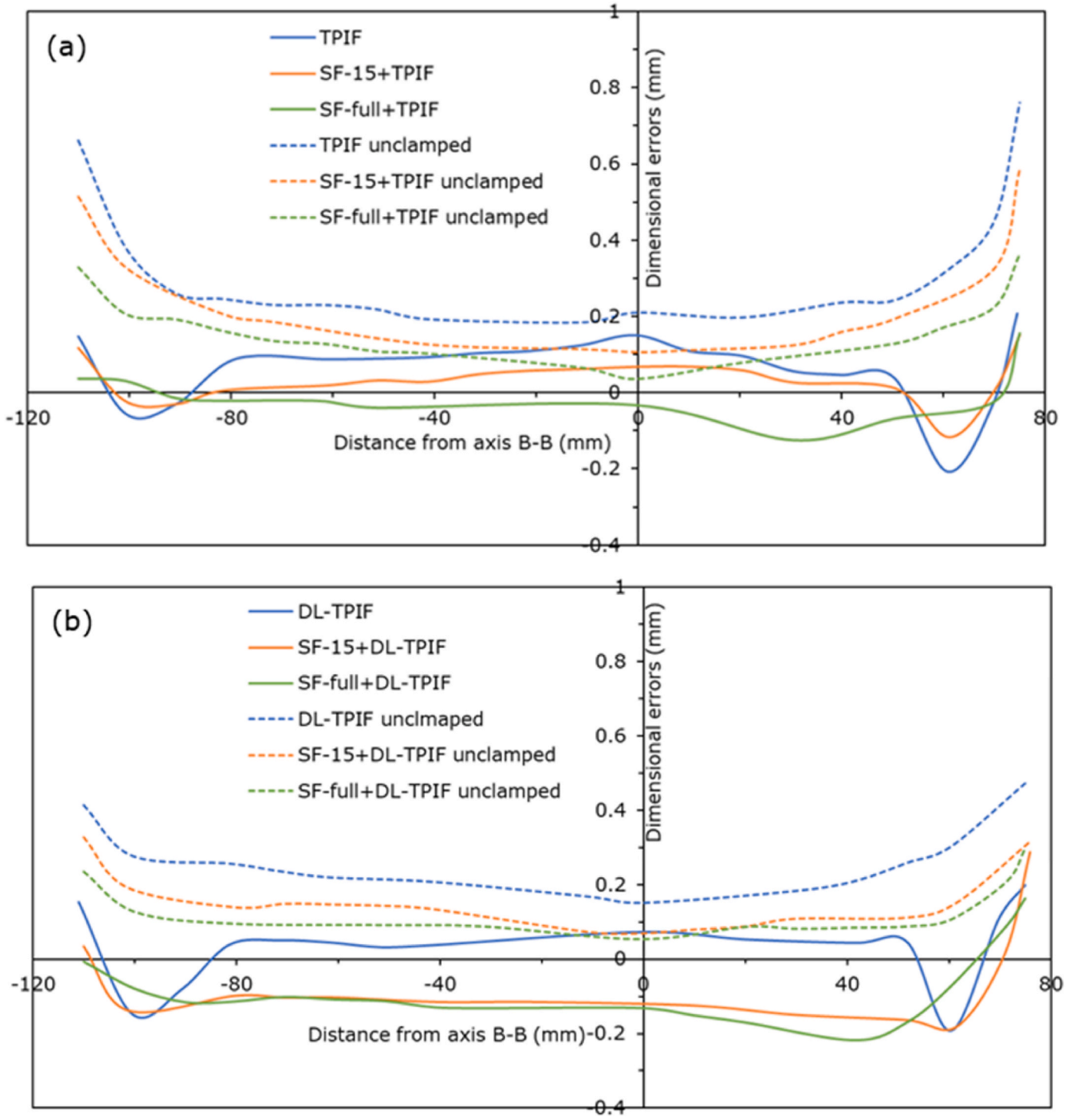

Fig. 32. Dimensional errors of parts before and after unclamping (a) the hybrid SF and TPIF process, and (b) the hybrid SF and DL-TPIF process with different pre-stretching conditions.

DL-TPIF process were compared to those produced by the conventional TPIF process under the same pre-stretching conditions. Six forming processes were evaluated through experimental testing and FE analysis in terms of strain and stress distributions, thickness variations, and geometrical accuracy. The main conclusions can be drawn in the following.

1. The regions of maximum thinning regions are different in the stretch forming and TPIF (or DL-TPIF) processes. As a result, a more even thickness distribution was achieved using the hybrid stretch forming and the TPIF or DL-TPIF processes than that made of the stretch forming process or conventional TPIF (or DL-TPIF) individually.
2. The proposed DL-TPIF process can reduce sheet thinning and obtain a uniform thickness distribution. When combined with the stretch forming process, these effects became more remarkable as the pre-stretching depth increased. In the case of a dome shape with a maximum 57° draw angle, the initial thickness was 0.8 mm. The minimum thickness was 0.69 mm for the part produced by the hybrid stretch forming and DL-TPIF process, which was equivalent to a

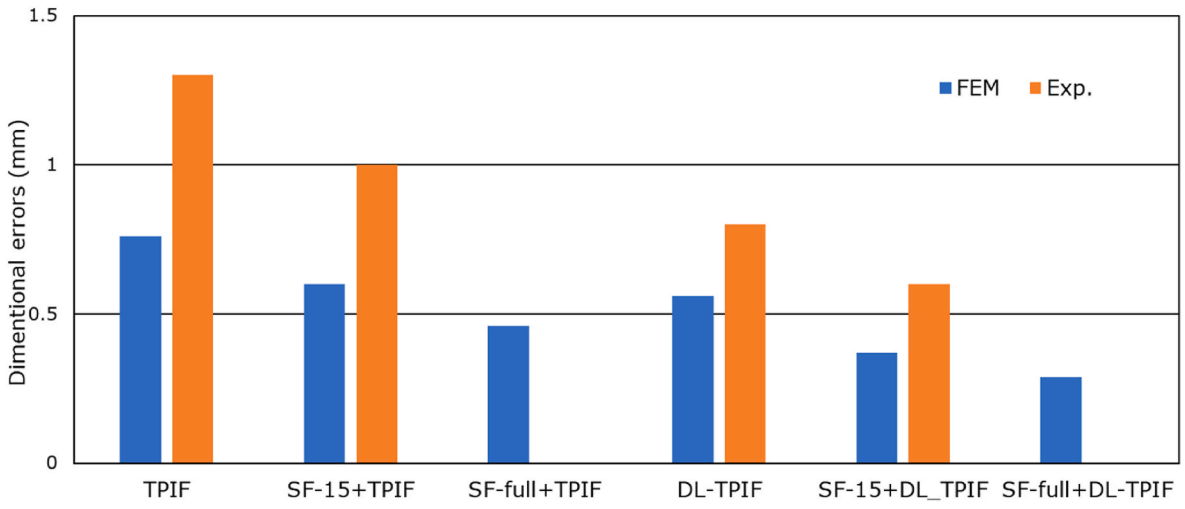

Fig. 33. Comparisons of the maximum dimensional errors between the FE predicted and experimental testing results for the irregular shape.

thickness reduction of 13.8%. This value was less than a third of the thickness reduction in the conventional TPIF process (45%).

3. The overall geometrical accuracy of the DL-TPIF process was better than that obtained by the TPIF process. This could be explained by the use of the upper dummy sheet to apply more constraints to the target blank sheet.
4. By increasing the pre-stretching depth, a more accurate part could be produced by both the TPIF and DL-TPIF processes. After conducting the stretch forming process, the blank sheet was under tension. The applied tension could reduce the stress difference between the top and bottom elements to reduce the degree of springback. Hence, the hybrid stretch forming and TPIF (or DL-TPIF) processes provided a favourable condition of sheet deformation for improved geometrical accuracy.

Declaration of competing interest

The authors declare that they have no known competing financial interests or personal relationships that could have appeared to influence the work reported in this paper.

Acknowledgements

This work was partly supported by the Engineering and Physical Sciences Research Council [grant number EP/W010089/1].

References

[1] Duflou JR, Habraken A-M, Cao J, Malhotra R, Bambach M, Adams D, Vanhove H, Mohammadi A, Jeswiet J. Single point incremental forming: state-of-the-art and prospects. Int J Material Form 2018;11:743–73. https://doi.org/10.1007/s12289-017-1387-y.

[2] Peng W, Ou H, Becker A. Double-sided incremental forming: a review. J Manuf Sci Eng 2019;141(5):1–12. https://doi.org/10.1115/1.4043173.

[3] Zhu H, Ou H, Popov A. Incremental sheet forming of thermoplastics: a review. Int J Adv Des Manuf Technol 2020;111(1):565–87. https://doi.org/10.1007/s00170-020-06056-5.

[4] Peng W, Ou H. Deformation mechanisms and fracture in tension under cyclic bending plus compression, single point and double-sided incremental sheet forming processes. Int J Mach Tool Manufact 2023;184:1–21. https://doi.org/10.1016/j.ijmachtools.2022.103980.

[5] Araghi BT, Manco G, Bambach M, Hirt G. Investigation into a new hybrid forming process: incremental sheet forming combined with stretch forming. CIRP annals 2009;58(1):225–8. https://doi.org/10.1016/j.cirp.2009.03.101.

[6] Attanasio A, Ceretti E, Giardini C, Mazzoni L. Asymmetric two points incremental forming: improving surface quality and geometric accuracy by tool path optimization. J Mater Process Technol 2008;197(1–3):59–67. https://doi.org/10.1016/j.jmatprotec.2007.05.053.

[7] Taleb Araghi B, Göttmann A, Bambach M, Hirt G, Bergweiler G, Diettrich J, Steiners M, Saeed-Akbari A. Review on the development of a hybrid incremental sheet forming system for small batch sizes and individualized production. J Inst Eng Prod 2011;5(4):393–404. https://doi.org/10.1007/s11740-011-0325-y.

[8] Kumar SP, Elangovan S, Mohanraj R, Boopathi S. Real-time applications and novel manufacturing strategies of incremental forming: an industrial perspective. Mater Today Proc 2021;46:8153–64. https://doi.org/10.1016/j.matpr.2021.03.109.

[9] Ben Said L. The incremental sheet forming; technology, modeling and formability: a brief review. Proc IME E J Process Mech Eng 2022;236(6):2729–55. https://doi.org/10.1177/09544089221093306.

[10] Taleb-Araghi B, Goettmann A, Bambach M, Biermann T, Hirt G, Weisheit A. Development of hybrid incremental sheet forming processes. In: International conference on metal forming; 2010. p. 918–21.

[11] Choi H, Lee C. A mathematical model to predict thickness distribution and formability of incremental forming combined with stretch forming. Robot Comput Integrated Manuf 2019;55:164–72. https://doi.org/10.1016/j.rcim.2018.07.014.

[12] Taleb Araghi B, Göttmann A, Bergweiler G, Saeed-Akbari A, Bültmann J, Zettler J, Bambach M, Hirt G. Investigation on incremental sheet forming combined with laser heating and stretch forming for the production of lightweight structures. In: Key engineering materials. Trans Tech Publ; 2011. p. 919–28.

[13] Lora FA, Fritzen D, Alves de Sousa R, Schaffer L. Studying formability limits by combining conventional and incremental sheet forming process. Chin J Mech Eng 2021;34(1):1–12.

[14] Lu B, Zhang H, Xu D, Chen J. A hybrid flexible sheet forming approach towards uniform thickness distribution. Procedia CIRP 2014;18:244–9. https://doi.org/10.1016/j.procir.2014.06.139.

[15] Zhang H, Lu B, Chen J, Feng S, Li Z, Long H. Thickness control in a new flexible hybrid incremental sheet forming process. Proc IME B J Eng Manufact 2017;231(5):779–91. https://doi.org/10.1177/0954405417694061.

[16] Skjoedt M, Bay N, Ingarao BE. Single point incremental forming using a dummy plate-multiplate forming. In: 2nd international conference on new forming technology, bremen; 2007.

[17] Chang Z, Chen J. Investigations on the deformation mechanism of a novel three-sheet incremental forming. J Mater Process Technol 2020;281:1–10. https://doi.org/10.1016/j.jmatprotec.2020.116619.

[18] Chang Z, Chen J. Investigations on the forming characteristics of a novel flexible incremental sheet forming method for low-ductility metals at room temperature. J Mater Process Technol 2022;301:1–10. https://doi.org/10.1016/j.jmatprotec.2021.117456.

[19] Zhao X, Ou H. A new flexible multi-point incremental sheet forming process with multi-layer sheets. J Mater Process Technol 2023:1–15. https://doi.org/10.1016/j.jmatprotec.2023.118214.

[20] Xiaoqiang L, Kai H, Xu S, Haibo W, Dongsheng L, Yanle L, Qing L. Experimental and numerical investigation on surface quality for two-point incremental sheet forming with interpolator. Chin J Aeronaut 2020;33(10):2794–806. https://doi.org/10.1016/j.cja.2019.11.011.

[21] Duchêne L, Guzmán CF, Behera AK, Duflou JR, Habraken AM. Numerical simulation of a pyramid steel sheet formed by single point incremental forming using solid-shell finite elements. In: Key engineering materials. Trans Tech Publ; 2013. p. 180–8.

[22] Aerens R, Eyckens P, Van Bael A, Duflou J. Force prediction for single point incremental forming deduced from experimental and FEM observations. Int J Adv Des Manuf Technol 2010;46(9):969–82. https://doi.org/10.1007/s00170-009-2160-2.

[23] Fang Y, Lu B, Chen J, Xu D, Ou H. Analytical and experimental investigations on deformation mechanism and fracture behavior in single point incremental forming. J Mater Process Technol 2014;214(8):1503–15.

[24] Li Y, Daniel WJ, Meehan PA. Deformation analysis in single-point incremental forming through finite element simulation. Int J Adv Des Manuf Technol 2017;88(1):255–67. https://doi.org/10.1007/s00170-016-8727-9.

[25] Shin J, Bansal A, Chang R, Taub A, Banu M. Process planning for precision incremental forming of complex parts. In: AIP conference proceedings. AIP Publishing LLC; 2019. p. 1–7.
[26] Behera AK, Lu B, Ou H. Characterization of shape and dimensional accuracy of incrementally formed titanium sheet parts with intermediate curvatures between two feature types. Int J Adv Des Manuf Technol 2016;83:1099–111. https://doi.org/10.1007/s00170-015-7649-2.
[27] Lu B, Ou H, Shi S, Long H, Chen J. Titanium based cranial reconstruction using incremental sheet forming. Int J Material Form 2016;9(3):361–70. https://doi.org/10.1007/s12289-014-1205-8.
[28] Lu H, Liu H, Wang C. Review on strategies for geometric accuracy improvement in incremental sheet forming. Int J Adv Des Manuf Technol 2019;102(9):3381–417. https://doi.org/10.1007/s00170-019-03348-3.
[29] Pohlak M, Küttner R, Majak J, Karjust K, Sutt A. Experimental study of incremental forming of sheet metal products. In: Proc of the fourth international DAAAM conference. Tallinn, Estonia: Citeseer; 2004. p. 139–42.